CONFIDENTIAL

NATIONAL AERONAUTICS AND SPACE ADMINISTRATION
CONTRACT NO. NASw-6

GROUP 4
Downgraded at 3 year intervals; declassified after 12 years

Quarterly Summary Report No. 38-4

for the period April 1, 1961 to June 31, 1961

Copy No._____

JET PROPULSION LABORATORY
CALIFORNIA INSTITUTE OF TECHNOLOGY
PASADENA, CALIFORNIA

July 15, 1961

CONFIDENTIAL

27 PAGES

Preface

This report is a quarterly summary of the research activities conducted by the Jet Propulsion Laboratory in the field of nondestructive testing of solid-propellant rocket motors. Section I presents a general description of the subject areas covered by the entire program; Section II details the progress in specific areas of research. An introduction to the problems and objectives of the program was given in *QSR 38-1*, and a bibliography of the subject is presented in *QSR 38-1*, *-2*, and *-3*.

The work reported herein is undertaken in partial fulfillment of the Advanced Research Projects Agency Letter Order No. 107-60, for the National Aeronautics and Space Administration.

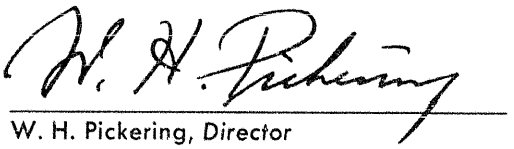

W. H. Pickering, *Director*
Jet Propulsion Laboratory

This document contains information affecting the national defense of the United States, within the meaning of the Espionage Laws, Title 18, U.S.C., Sections 793 and 794, the transmission or revelation of which in any manner to an unauthorized person is prohibited by law.

Quarterly Summary Report No. 38-4

Copyright © 1961
Jet Propulsion Laboratory
California Institute of Technology

Contents

I. Introduction 1

II. Physical Properties Studies 2

A. Motor Strain Testing
by C. H. Lewis, Jr. 2

B. Influence of Strain on Burning Rate
by J. Coy 5

C. Viscoelastic Strain Analysis by Photoelastic Coating Technique, II
by A. San Miguel 6

D. Polymer Degradation Mechanisms
by J. D. Ingham and N. S. Rapp 16

E. Homogeneity of Polyurethane Propellants
by A. J. Havlik and J. Moacanin 20

References 23

I. INTRODUCTION

In future issues of the *QSR* the status of all nondestructive testing programs will be reported whether they are active or inactive. The entire program qualitatively covers the following areas: (a) an examination of the methods for determining mechanical properties and of the factors which influence the results obtained, (b) a comparison of resin with propellant properties to determine the extent to which the properties can be determined from the resin (broadly termed rheological studies per se); (c) studies of degradation mechanism in polyurethanes, and (d) an examination of the behavior of propellants in realistic geometries or actual motors.

Current test methods and procedures are being examined for sources of error in determining mechanical properties. This work includes considerations of the homogeneity of the sample itself, the sample size and the sample preparation, sample handling prior and during testing, and the measurement of strain in a standard tensile test. Additional tests will be developed, such as the measurement of Poisson's ratio or shear in torsion, and sonic or triaxial testing.

In addition to comparisons of resin with propellant, efforts will be extended to studies on the effect of the volumetric loading of fillers on mechanical properties, theories of propellant and resin failure, and studies on finite deformation behavior to determine the stored energy function W for resins and propellants. It should be recognized, of course, that it will be difficult to discriminate between the development of tests intended to distinguish between propellants and that intended to advance or test the theory of rheological behavior.

The mechanism of degradation is being studied for polyurethanes, since this knowledge is required to understand the phenomena, to provide a chemical method of following the degradation if possible, and to correlate specifically the observed mechanical property changes with the chemical changes on degradation.

All of these factors will be important to the analysis of failure modes in motors. The motor test program currently consists of measurements of the strain developed in a pressurized case-bonded cylinder for comparison with the theoretical behavior of such motors, studies of the surface strains developed in realistic motor configurations using a photostress technique, and the measurement of the burning rate of strained propellant as a function of strain. Work is now in progress to determine critical void size in motor grains and the effect of grain anomalies on motor performance.

II. Physical Properties Studies

A. Motor Strain Testing

C. H. Lewis, Jr.

The probe mentioned in *QSR 38-1*, Page 23, for detecting the change in inner diameter of propellant grain has been constructed and tested. The probe (Fig 1) consists of a pivoted beam with a steel ball on one end which rests against the propellant inner surface. The other end of the beam is attached to the movable core of a differential transformer set into the probe base. The base is located by pins in the end cap such that the movable core of the transformer is in the most linear region for each mandrel size and, in addition, the beam pivot is placed so that the ball end of the beam contacts the propellant in the center of the longitudinal axis of the test chamber. The small spring holds the beam against the propellant surface with approximately a 2-gm force at the ball end.

Excitation of the transformer is done with a Wiancko system (Fig 2). The sensitivity of this system is such that it is possible to detect movements of as little as 0.0002 in. over a range of 0.020 in. and still monitor movements of up to 0.250 in. Calibration of the probe in done in a jig (Fig 3), which is a replica of the end and inside geometry of the test chamber. The ball is positioned by a micrometer depth gage in a slot that is precisely located with respect to the center line of the chamber.

Testing of motors has begun using this device; strain gages were placed on the outside of the test chambers to detect the displacements of the outside surface (Fig 4). Six motors have been tested to date: two each at $(b/a)^2$ of 6.9, 10, and 25. The results of these tests are shown in Figure 5 where the percentage change of the inner radius is plotted against $(b/a)^2$. Also shown is the

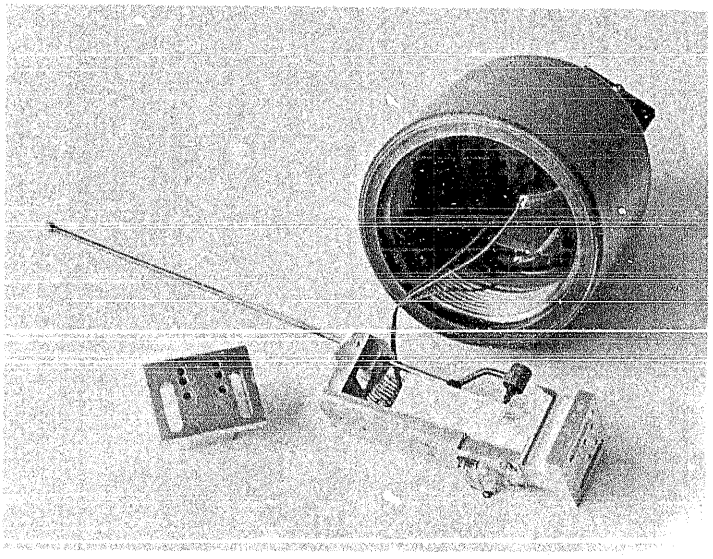

Figure 1. Probe for detecting inner-surface radial displacements

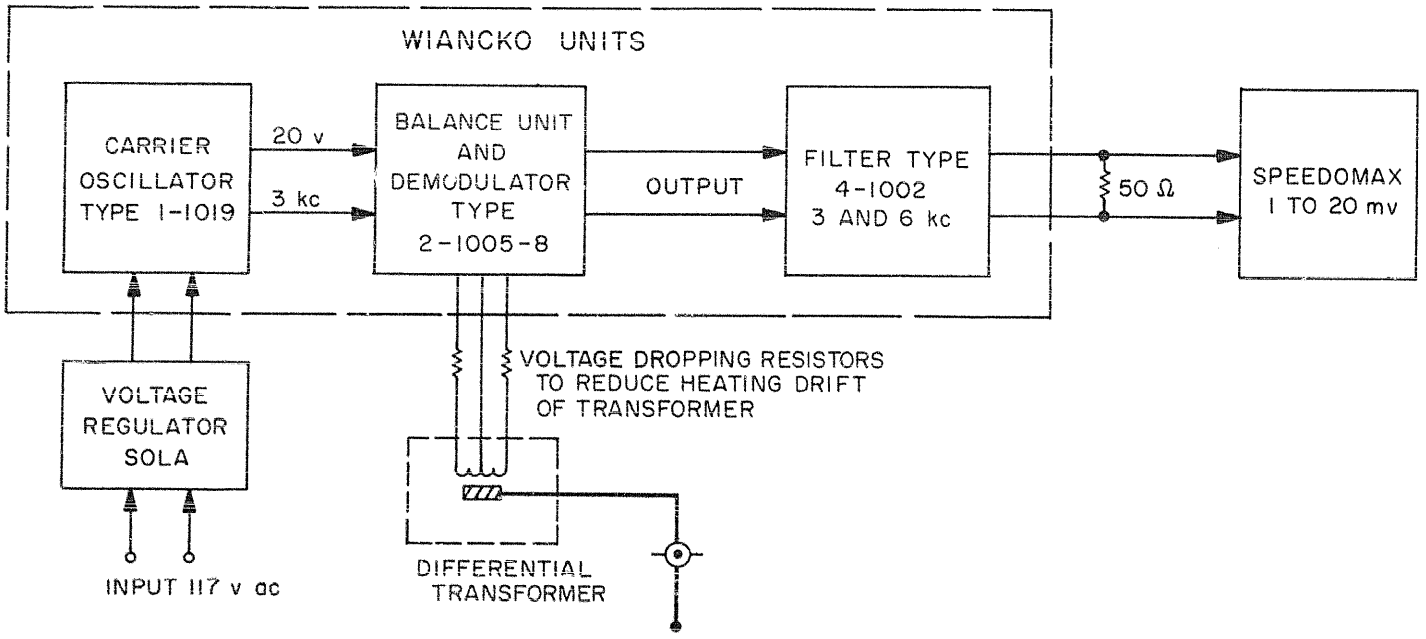

Figure 2. Instrumentation system for probe

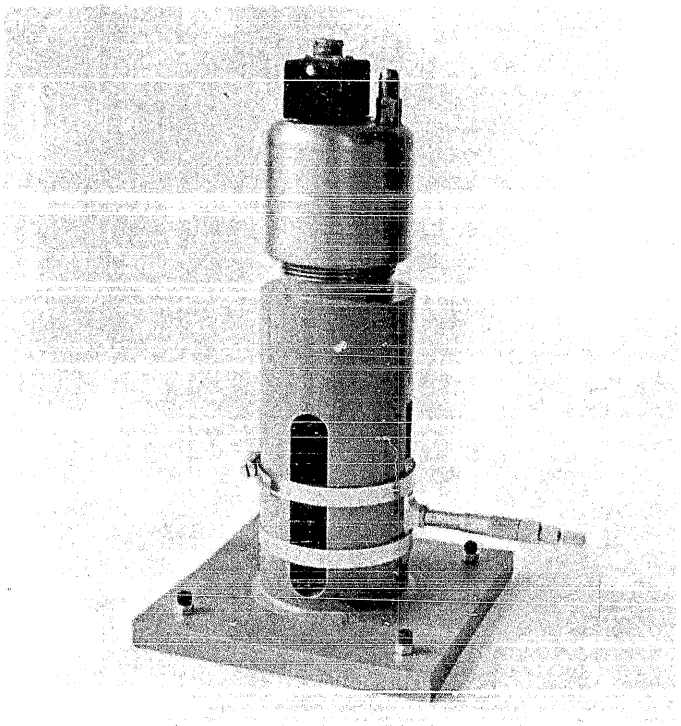

Figure 3. Calibration jig for probe

change in radius that would result if the inner surface deformed with respect to the case deformation in a geometrically similar manner and with no change in volume of the propellant.

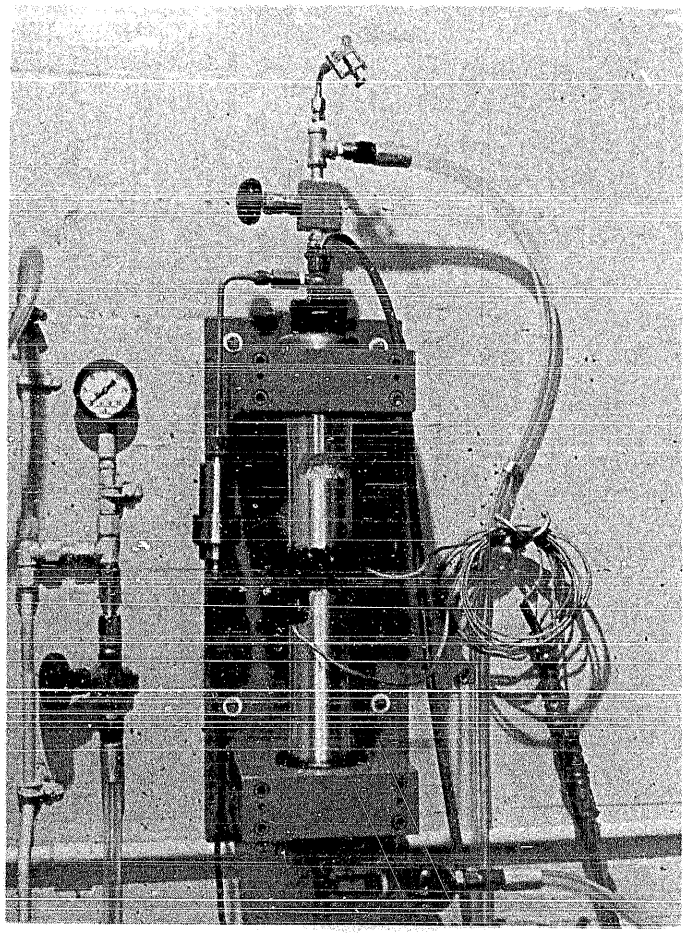

Figure 4. Displacement measuring setup

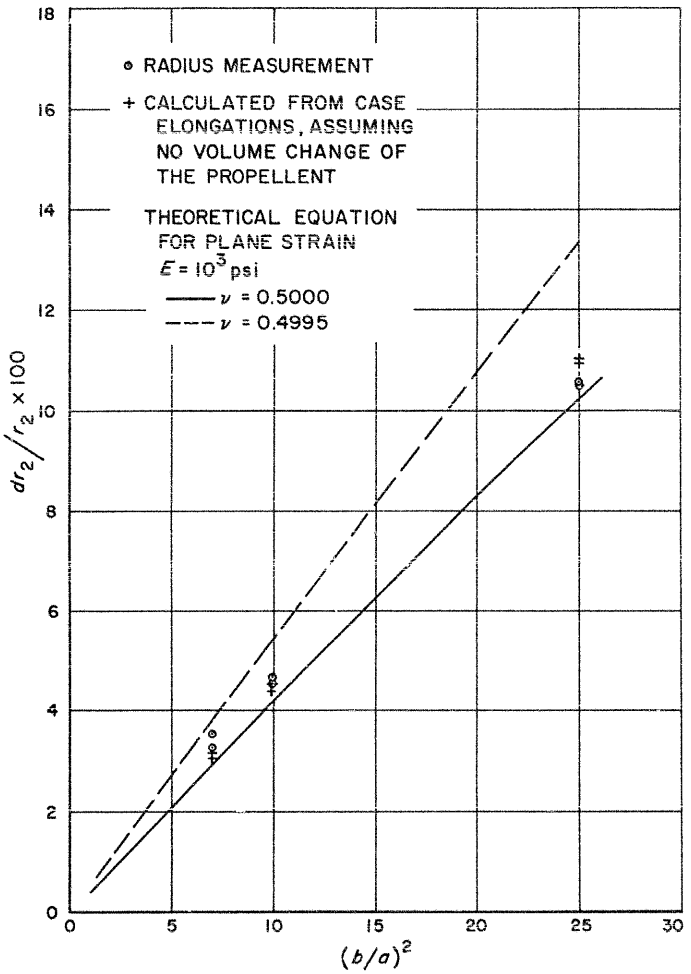
RADIUS MEASUREMENT
+ CALCULATED FROM CASE ELONGATIONS, ASSUMING NO VOLUME CHANGE OF THE PROPELLENT
THEORETICAL EQUATION FOR PLANE STRAIN
E = 10^3 psi
ν = 0.5000
ν = 0.4995
dr2/r2 × 100
(b/a)^2

Figure 5. Test results normalized to 1600 psi

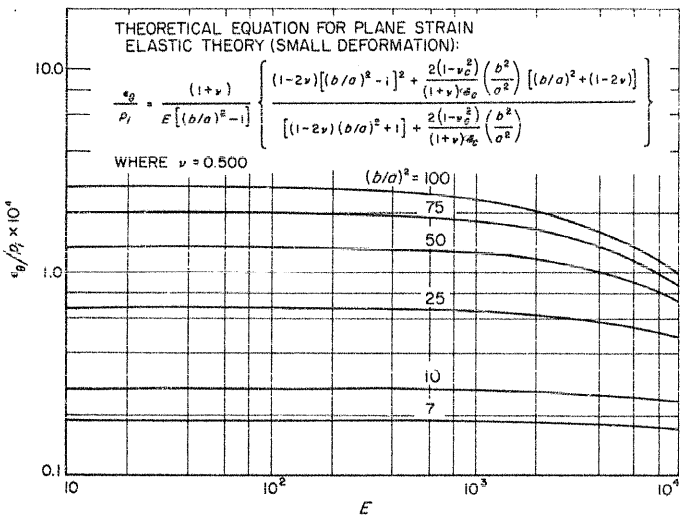

Figure 6. Theoretical tangential strain as a function of propellant modulus

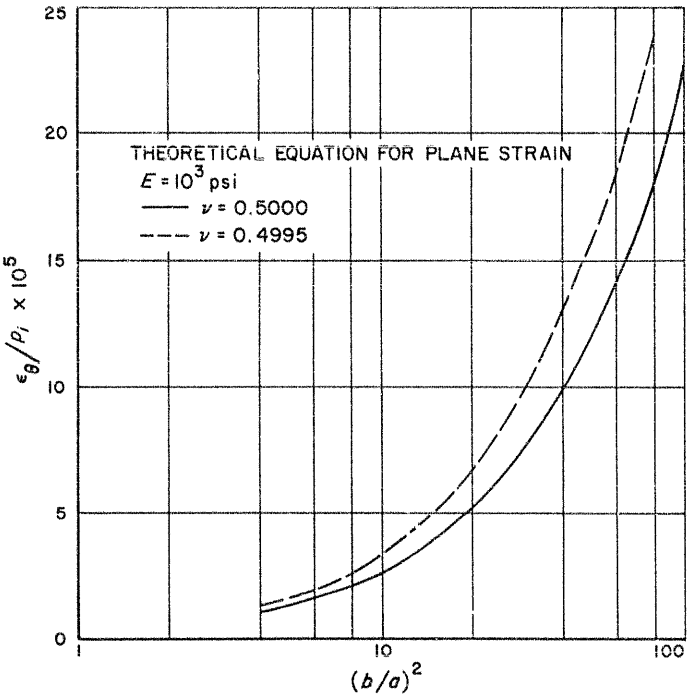

Figure 7. Tangential strain at inner periphery as a function of web ratio

The calculated radius change agrees reasonably well with the directly measured one. These points can be bracketed by curves derived from small deformation elastic theory for plane strain of an internally pressurized case-bonded propellant grain (*QSR 38-1*, Equation 19, p 22) using $E = 10^3$ psi, and ν propellant of 0.5000 and 0.4995. The actual modulus of this propellant in uniaxial tension at the strain rates of this experiment is of the order of 600 psi. However, Figure 6 shows that the effect of propellant modulus on inside strain should be small—below $E = 10^3$ psi for motors with $(b/a)^2 \leq 25$, and a $\nu = 0.500$. In addition, the effect of hydrostatic pressure will probably tend to increase the modulus in tension (Ref 1).

Tests will be made covering a range of $(b/a)^2$ from 7 to 100 at strain rates, calculated at the inner surface, up to 100%/min. For $(b/a)^2 > 50$, strains in excess of 20% will be obtained during some part of the test (Fig 7). Since the propellant to be used goes through maximum load at about 20% elongation in uniaxial tension, it is expected that failure will occur in some of these motors and that the initiation of cracks will be detected by the inside diameter measuring probe. Information as to the reinforcing effect of hydrostatic pressure could be obtained from this type of test.

B. Influence of Strain on Burning Rate

J. Coy

It has been shown that strain, applied parallel to a polyurethane propellant burning surface, can produce an increase in burning rate (*QSR* 38-2). Data have been extended to include another polyurethane propellant, having different mechanical and ballistic properties, and an additional condition of strain.

Propellant under tensile deformation is subjected to changes in geometry which can be expressed as a function of Poisson's ratio. Thus, one of the propellants used in this study (having a Poisson's ratio of 0.415) would have a lateral contraction of 4.15% perpendicular to the burning surface on application of a 10% tensile strain parallel to the burning surface and, consequently, the effective burning rate of the propellant should increase by 4.15%. The purpose of this study is to study the influence of strain on burning properties of propellant; therefore, in measuring the effect of strain on burning rate, it is necessary to correct for lateral contraction of a propellant specimen in order to measure true changes in burning rate.

1. Equipment and Procedure

The device used for straining propellant specimens and the method used for acquiring data were described in *QSR* 38-2. Some modifications are described in the following.

a. Specimen. The propellant specimen gage length has been increased from 1.5 to 2.5 in.; this was done by discarding the dumbbell-type clamps and gluing the specimen ends to metal plates with a hard epoxy resin. The increased gage length provides greater uniformity of strain in the center of the specimen where burning rates are measured.

The specimen had been ignited by placing a nichrome wire under a slit made in the propellant with a knife and electrically heating the wire. The present technique uses the nichrome wire to ignite a sliver of propellant placed adjacent to the propellant surface. The sliver ignites the specimen without producing a discontinuity on the specimen surface.

b. Burning rate measurement. Burning rates were measured by measuring the time for wires (placed in holes centered 1 in. apart) to be consumed. The holes are now placed 1 in. plus one hole diameter apart. The lateral contraction (wire separation) is calculated as a function of tensile strain in determining burning rate.

c. Propellant. The propellant used in recent studies is a polyurethane formulation designated F39CS containing 2.0% aluminum, 1.75% lithium fluoride, and 76.6% ammonium perchlorate. This propellant has an initial modulus of elasticity, $E_0 = 1477$ psi at a strain rate of 0.74 min^{-1} and a burning rate exponent, $n = 0.033$ for pressures between 400 and 1000 psia. Propellant used in earlier studies and designated X-500-80 contains 80% ammonium perchlorate in a polyurethane binder; this propellant has an $E_0 = 714$ psi, and $n = 0.17$.

2. Discussion

a. Effect of strain on burning rate. The influence of strain on the burning rate as a function of pressure is shown in Figure 8. Strains of 0, 5, and 10% are shown for each of the two propellants studied. It is evident that the burning-rate/strain relationship is influenced by pressure; further, the influence is more pronounced in the case of smaller strains for the pressure range used. At pressures above 1000 psia, the influence of pressure on the burning rate of strained propellant apparently disappears, although the data do not extend to pressures sufficiently high to verify this assumption. At pressures less than 1000 psi the propellant strained to 5% undergoes a transitional increase in burning rate, and it may be assumed that at much lower pressures the propellant strained to 10% would do the same. This would imply that significant changes in burning mechanism or flame structure occur only during the transition pressure region for a given strain. The increase in burning rate at 1000 psi is 1.2 to 1.5% for each percent of strain for both propellants.

b. Effect of prestraining on burning rate. The influence of prestraining on burning rate may be shown from the data in Table 1. Propellant specimens were tested as previously described at 0 and 10% strain, igniting the propellant 12 sec after pressurizing and straining. Two additional conditions were introduced to study the effect of time on the specimens; these specimens were ignited 20 min after straining with pressurization accomplished both before and after the 20-min period. After straining to 10%, the propellant had a stress of 76 psi; 20 min after straining, the stress had dropped to 43 psi. Data from Table 1 indicate that the burning rate changes only as a function of strain at a given pressure and not as a function of prestraining or long-term pressure history.

c. Precision of data. The standard deviation of burning rate data from the device is ± 0.0093 in./sec or less than

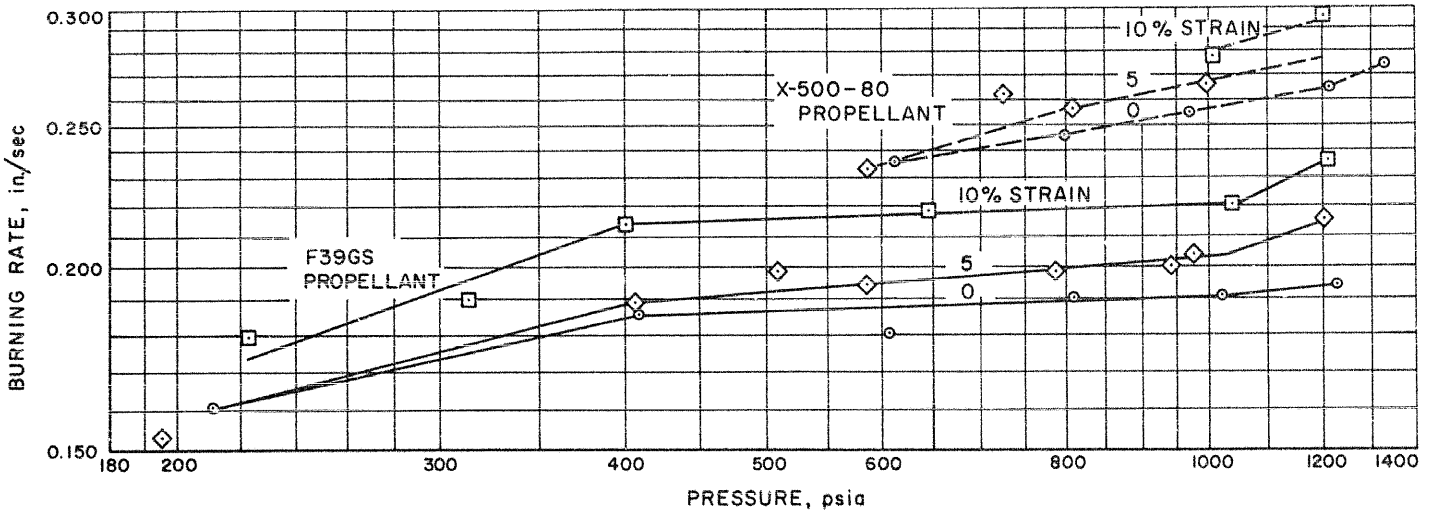

Figure 8. Effect of strain on burning rate as a function of pressure

±5% at a burning rate of 0.20 in./sec. Although the measured burning length of the specimens was only 1 in., the precision of data from the device compares favorably with conventional strand burner data. The precision is adequate for the type of data required in this study.

3. Conclusions

The influence of pressure on the burning rate of strained propellant is pronounced in the pressure region of interest to the rocket designer. From the data presented no conclusion can be made concerning the mechanism involved. Examination of burning propellant being strained at constant pressure in a window bomb should demonstrate the effect clearly and provide some insight into the mechanism.

The absence of influence of prestraining on the burning rate is somewhat surprising when considering the viscoelastic nature of the propellant. This becomes significant when considering that propellant creep in a rocket motor may introduce large strains which permanently alter the ballistic performance of the rocket motor.

While the composite propellant system considered here used a polyurethane binder, it seems probable that the results would apply to other composite propellants. Double base systems would probably not be directly comparable because of their different binder structure and lower solids loading.

Table 1. Influence of prestraining on burning rate

Strain, %	Condition	Burning rate, in./sec	
		600 psia	1000 psia
0	—	0.191	0.193
10	a	0.212	0.211
10	b	0.211	0.215
10	c	0.211	0.213

a Ignited 12 sec after pressurizing and straining.
b Ignited 20 min after pressurizing and straining.
c Ignited 20 min after straining and immediately after pressurizing.

C. Viscoelastic Strain Analysis by Photoelastic Coating Technique, II

A. San Miguel

In *QSR 38-3*, a beam was chosen to illustrate the application of the photoelastic coating technique. It was noted that the coating material exhibited the same stress–optics properties in compression as it did in tension. The basic equipment and method of data reduction are being extended to more useful and practical strain measurements.

1. Apparatus and Procedure

Two geometries were chosen for study: a simple tubular (Fig 9) and a typical star (Fig 10) propellant grain. Both configurations were studied as external radially restricted and as free standing grains. The material being tested is an inert formulation whose physical properties

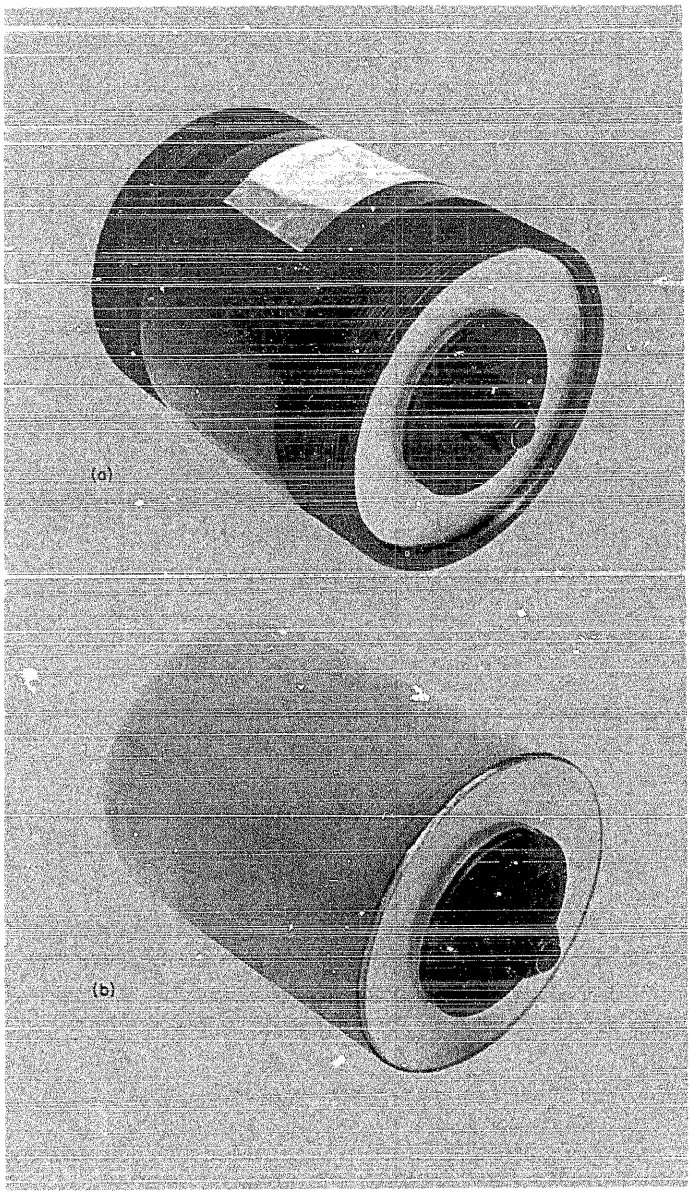

Figure 9. Assembled fixed (a) and free grain (b) tubular test specimens

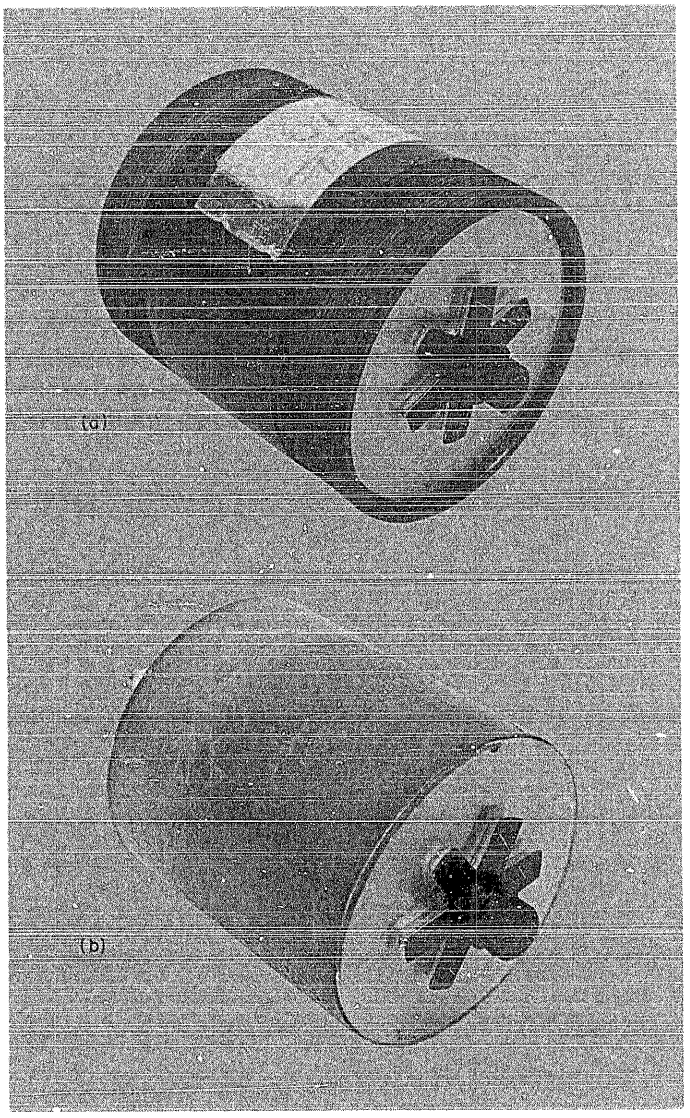

Figure 10. Assembled fixed (a) and free grain (b) star test specimens

are very similar to those of an operational polyurethane composite propellant. The dimensions of the test specimens are given in Figure 11.

Loading in all cases was accomplished by internal pressurization. The specimens were pressurized with nitrogen by use of a contoured latex bag, sealed to a shaft at both ends (Fig 12). The longitudinal expansion of the bag was controlled by means of adjustable end plates machined with a conical taper. This taper was required to compensate the specimen's internal radial expansion due to pressurization.

The specimen was vertically mounted in the test fixture (Fig 13). A two-dimensional loading was assured by constant adjustment of the axial position of the plates by the fixture during pressurization so that the bag could just be seen between the grain and the tapered end plate. The restrained grain consisted of the free grain inserted in a greased cylinder, permitting axial extension and minimizing any shear stresses. The data were recorded on colored film in the usual manner (Fig 14 and *QSR* 38-3).

2. *Birefringent Coating Material*

The birefringent coating material was calibrated in the usual way (Fig 15 and *QSR* 38-3). Enough resin was then

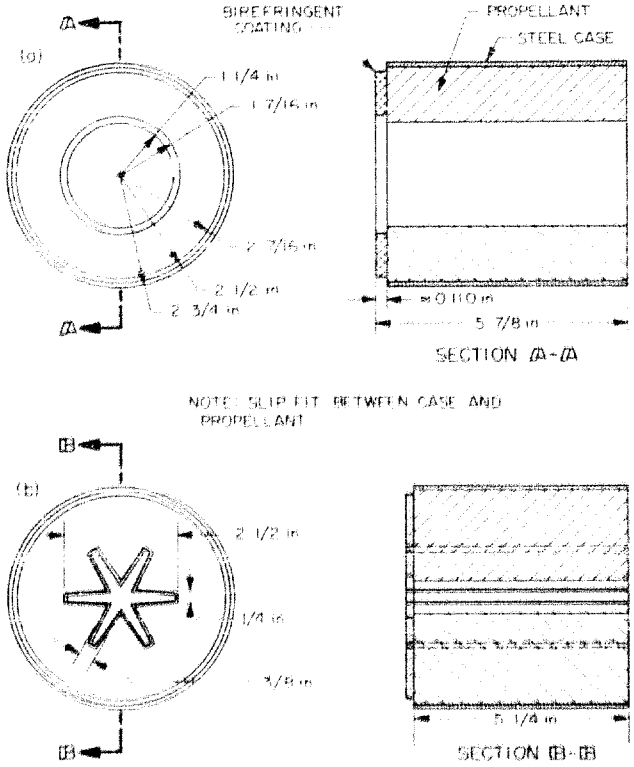

Figure 11. Dimensions of tubular (a) and star (b) test specimens

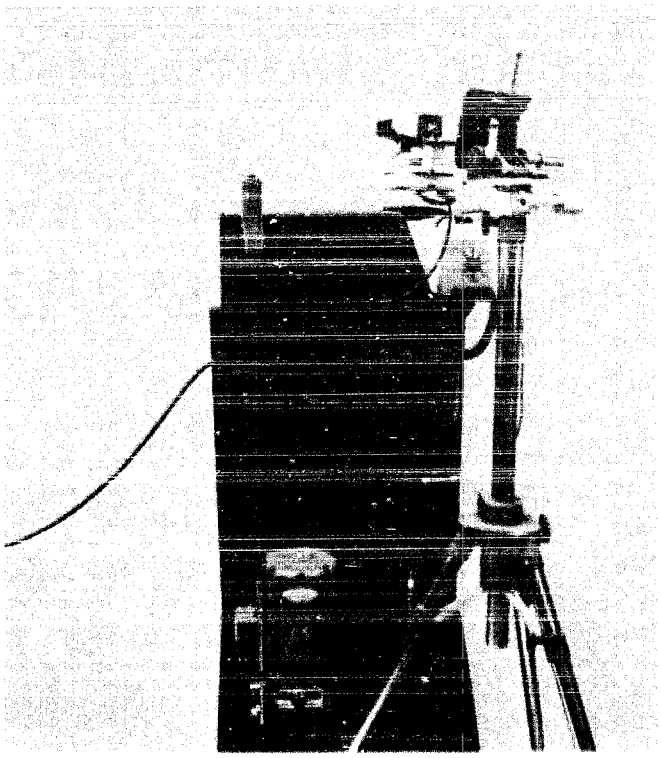

Figure 13. Specimen test fixture including camera polariscope

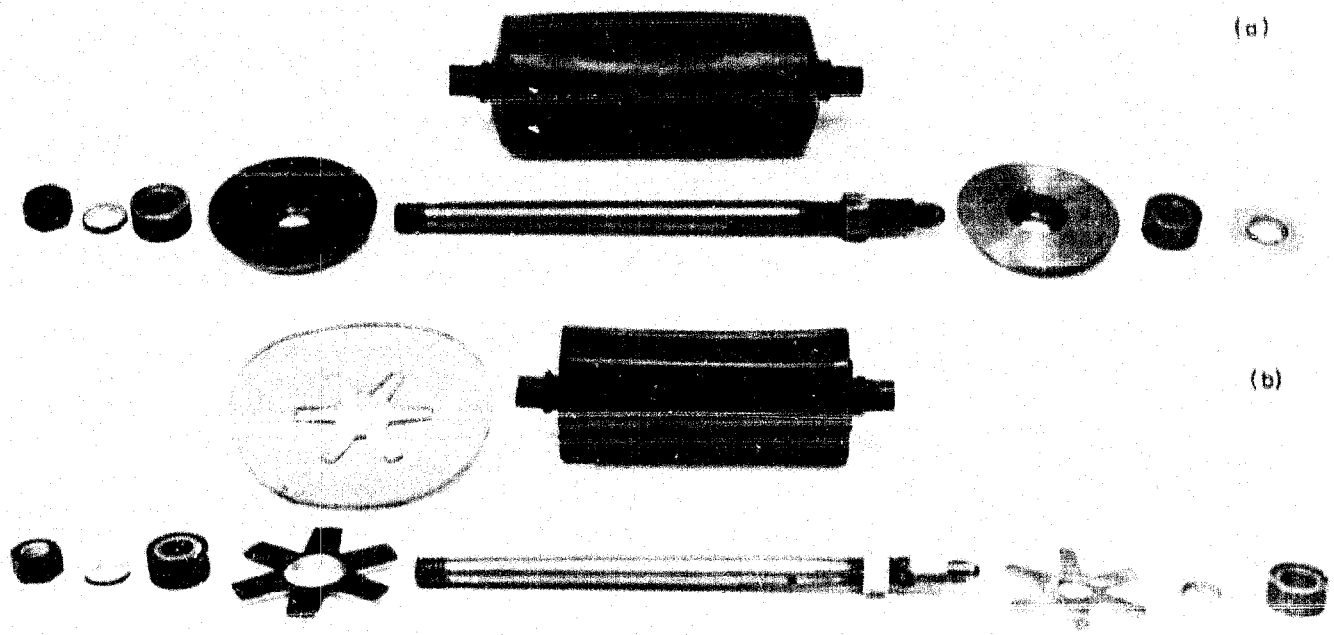

Figure 12. Pressurization assembly for tubular (a) and star (b) test specimens

Figure 14. Photographic polariscope data

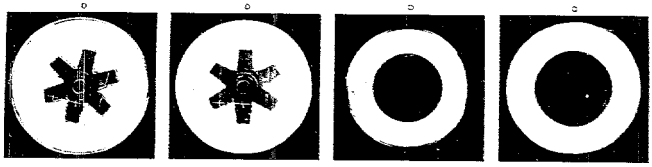

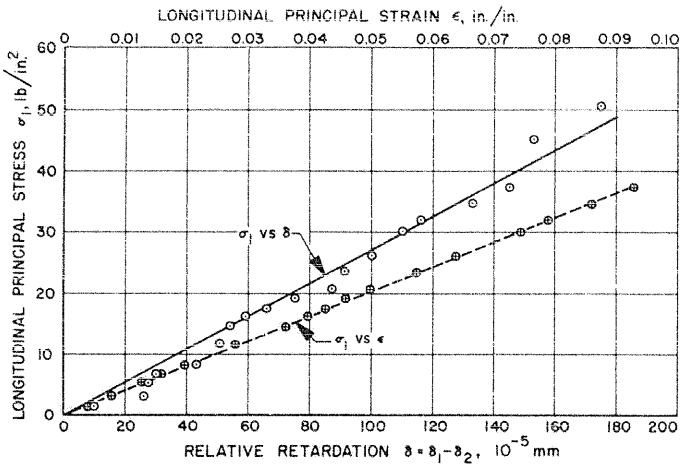
LONGITUDINAL PRINCIPAL STRAIN ε, in./in.
0 0.01 0.02 0.03 0.04 0.05 0.06 0.07 0.08 0.09 0.10
LONGITUDINAL PRINCIPAL STRESS σ1, lb/in.2
60 50 40 30 20 10 0
σ1 vs δ
σ1 vs ε
0 20 40 60 80 100 120 140 160 180 200
RELATIVE RETARDATION δ = δ1−δ2, 10−5 mm

Figure 15. Coating material calibration

cut to the required shape and bonded to the end of the grain (Fig 16) so that neither the end plate nor the metal cylinder would touch the coating.

3. Data Reduction

The range of pressures applied to the grains were 0 to 60 psi for the free standing grain and 0 to 150 psi for the contained grain. The isoclinic data are reduced from Figure 14 to Figure 17 for the two different grain configurations. Both geometries were traced from projected enlargements of a negative; six photographs were used to give a sufficient isoclinic distribution. All of the photographic data were acquired in 7 sec to minimize creep due to any viscoelastic effects.

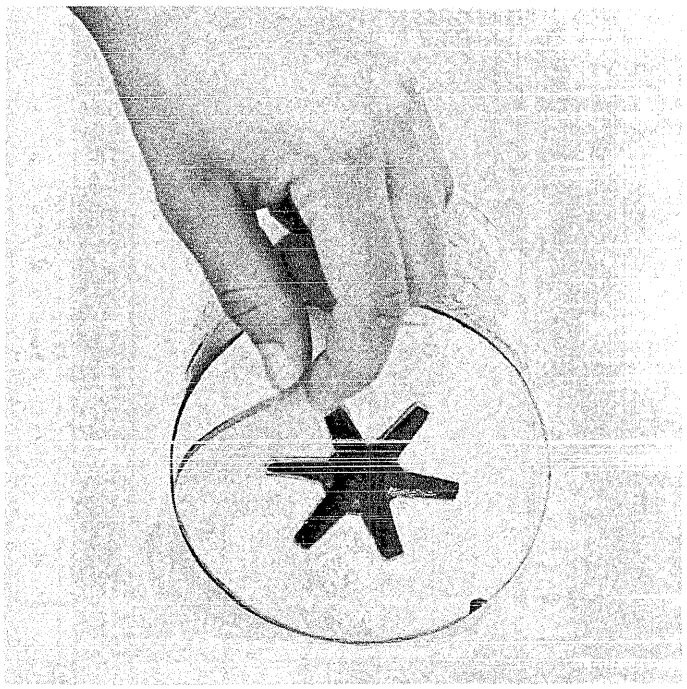

Figure 16. Coating material applied to end of specimen

By following the same procedures established in *QSR* 38-3 the principal strains were determined at arbitrarily chosen cuts. Figure 18 illustrates the graphical representation of the isochromatics for their corresponding geometry and loading (obtained from Fig 14 in the same manner used for Fig 17). In Figure 18, a plot in Cartesian coordinates of constant shear contours is superimposed upon the isochromatic plot. These shear contours are referenced with respect to the direction of the arbitrarily chosen cuts and polarizing angles. The nomograph and procedure used to separate the principal stresses may be found in *QSR* 38-3.

Table 2 summarizes the calculations that were necessary to reduce the difference in principal stresses $\sigma_1 - \sigma_2$ and σ_2 into principal strains in the coating material. Since the coating material was bonded to the grain, $E = 730$ psi, the strains in the grain were assumed to be that of the birefringent coating.

4. Theory

In *QSR* 38-3, it was found that for the given conditions a remarkably close agreement existed between measurements and theory. For purposes of comparison and prediction, the strain distribution across the web of the tubular grain has been derived analytically using small deformation elastic theory. Because of its geometric complexity, no attempt was made to treat the star-shaped configuration analytically.

The strain equations for a tubular grain were derived in Reference 2 and are as follows:

a. Free tubular grain, plane stress conditions.

$$\varepsilon_r = \frac{a^2 p_i}{(b^2 - a^2)E}\left[(1 - \nu) - (1 + \nu)\frac{b^2}{r^2}\right]$$

$$\varepsilon_\theta = \frac{a^2 p_i}{(b^2 - a^2)E}\left[(1 - \nu) + (1 + \nu)\frac{b^2}{r^2}\right]$$

where

ε_r = radial strain, in./in.
ε_θ = circumferential strain, in./in.
a = inner radius of tubular grain = 1.25 in.
b = outer radius of tubular grain = 2.50 in.
p_i = internal pressure = 60 psi
E = tensile modulus = 730 psi
ν = Poisson's ratio = 0.50 (assumed)
r = radial distance to point in tubular grain, in.

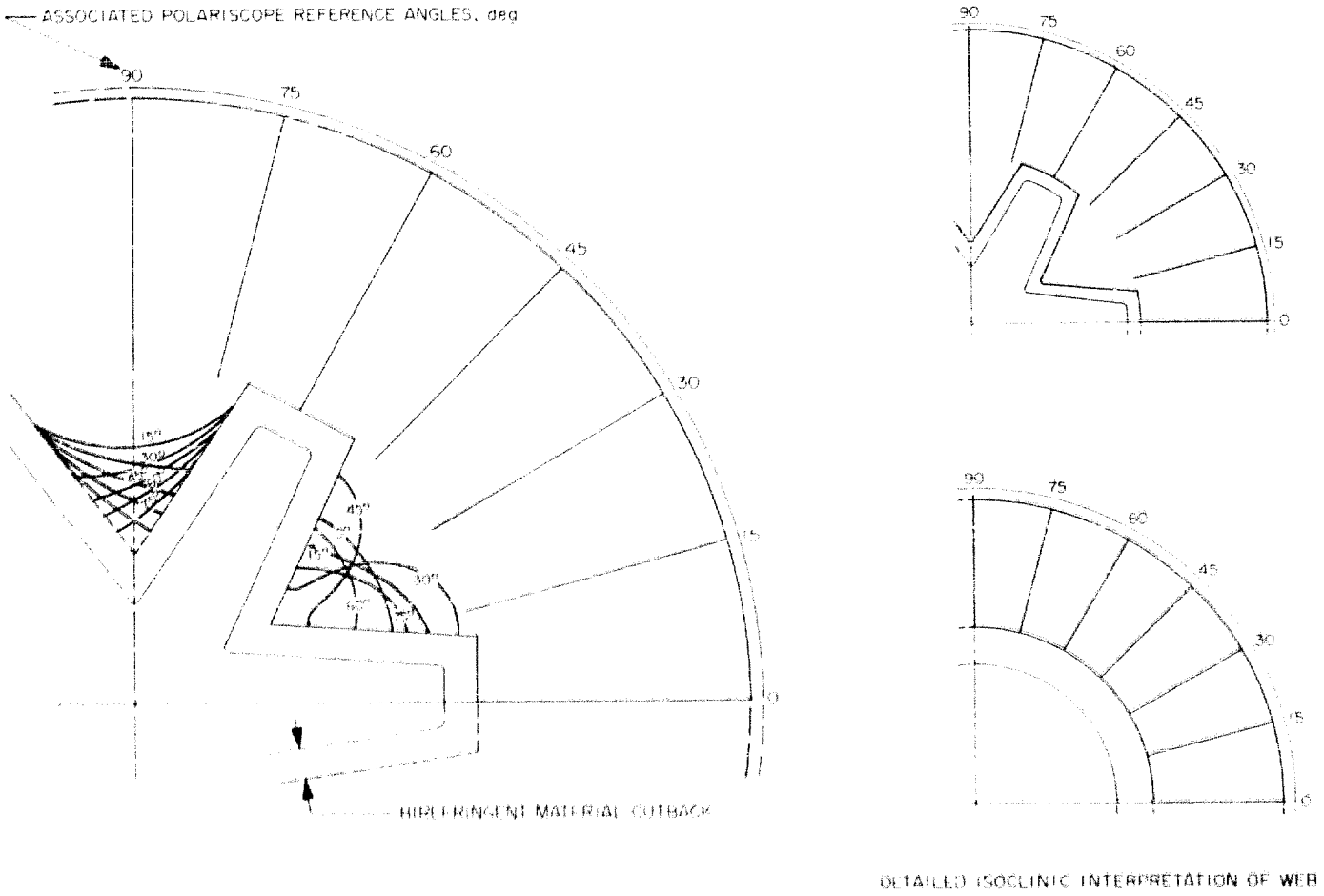

Figure 17. Graphical isoclinic interpretation of Figure 14

r	1.25	1.50	1.75	2.00	2.25	2.50
ϵ_θ	0.178	0.128	0.097	0.078	0.064	0.055
ϵ_r	0.151	0.100	0.070	0.050	0.037	0.027

b. Restrained tubular grain, plane stress conditions.

$$\epsilon_r = \frac{1}{(b^2 - a^2)E}\left[(1+\nu)a^2b^2(p' - p_i)\frac{1}{r^2} + (1-\nu)(p_i a^2 - p'b^2)\right]$$

$$\epsilon_\theta = \frac{1}{(b^2 - a^2)E}\left[-(1+\nu)a^2b^2(p' - p_i)\frac{1}{r^2} + (1-\nu)(p_i a^2 - p'b^2)\right]$$

where

$$p' = \frac{\dfrac{2a^2p_i}{(b^2-a^2)E}\left[(1+\nu_c)c^2 + (1-\nu_c)b^2\right]}{\left[(1+\nu)a^2 + (1-\nu)b^2\right] + \dfrac{(b^2-a^2)E}{(c^2-b^2)E_c}\left[(1+\nu_c)c^2 + (1-\nu_c)b^2\right]}$$

All symbols are the same except:

- p' — pressure at interface between grain and metal container, psi
- E_c — tensile modulus of metal containers — 30×10^6 psi
- ν_c — Poisson's ratio of metal container — 0.33
- c — outside radius of metal container — 2.75 in.

r	1.25	1.50	1.75	2.00	2.25	2.50
ϵ_θ	0.132	0.078	0.046	0.023	0.010	0.000
ϵ_r	0.220	0.166	0.134	0.113	0.098	0.090

5. Conclusion

Figure 19 graphically presents the discrepancies between small deformation elastic theory and experimen-

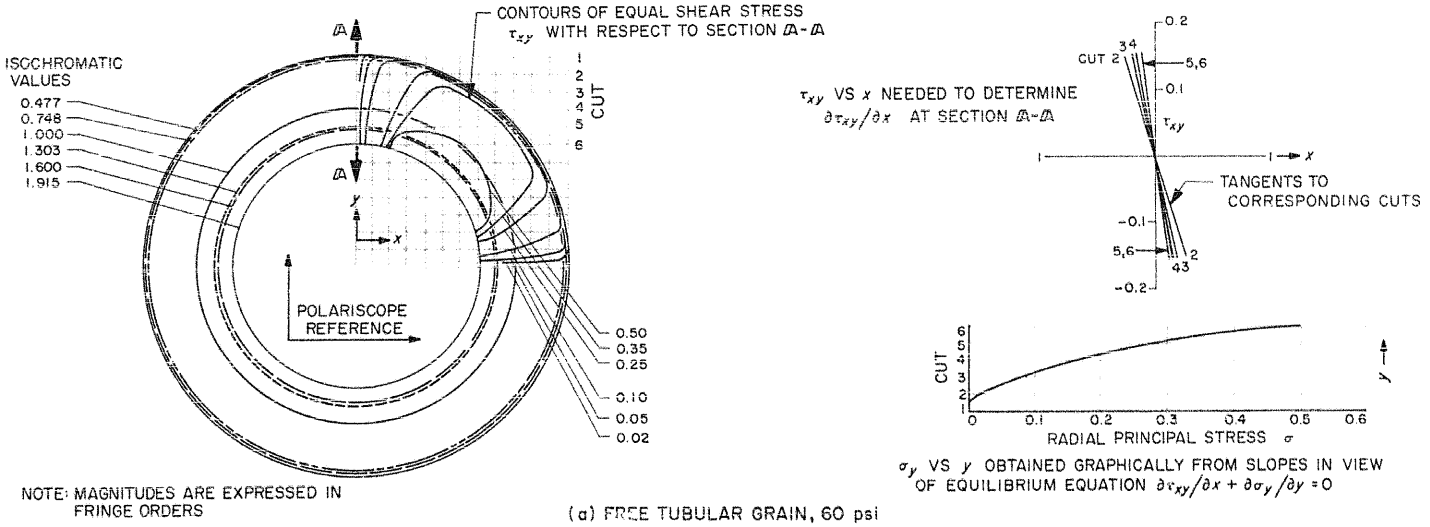

(a) FREE TUBULAR GRAIN, 60 psi

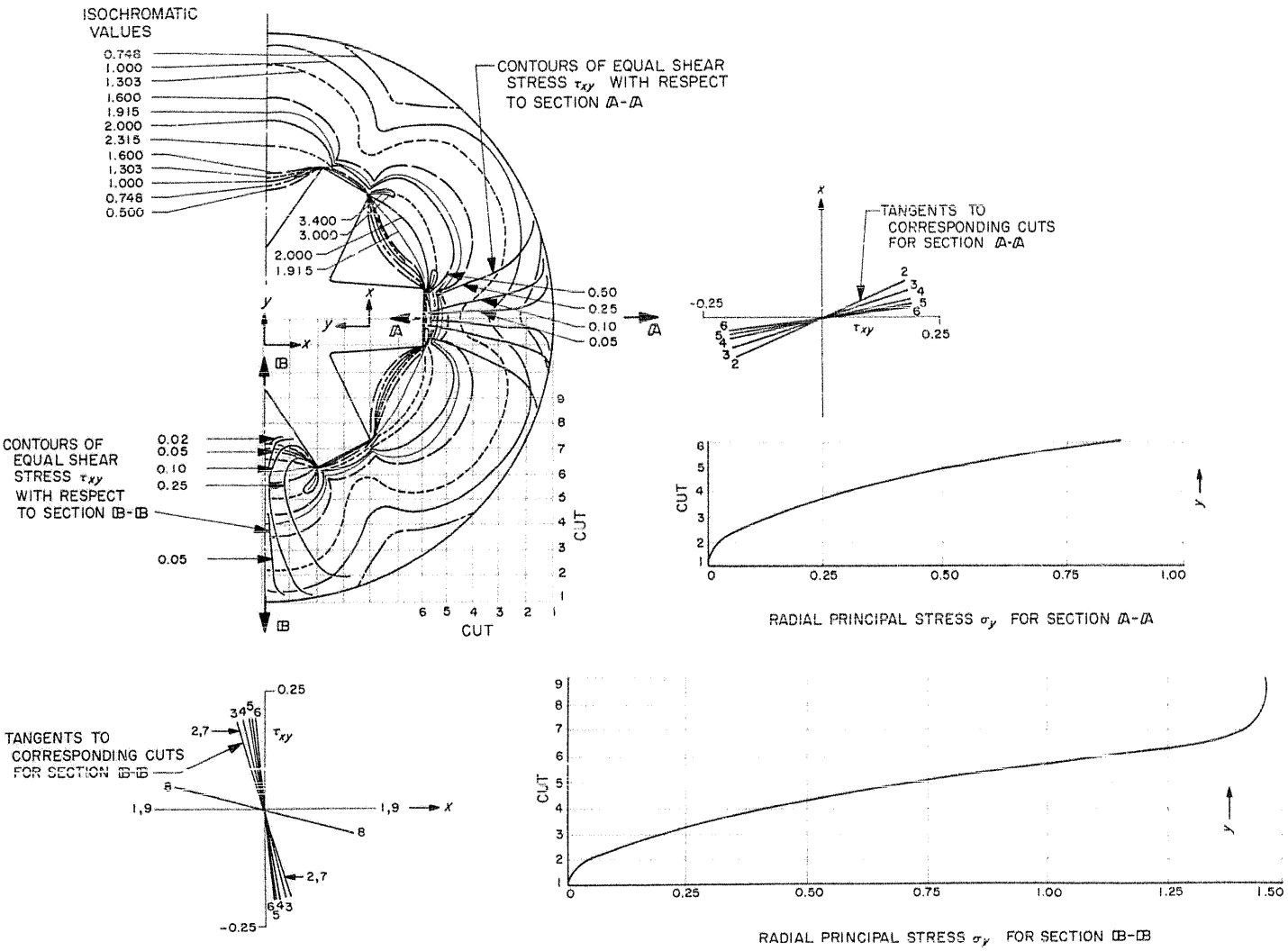

(c) FREE STAR GRAIN, 60 psi

Figure 18. Isochromatic distribution and separation of principal stresses

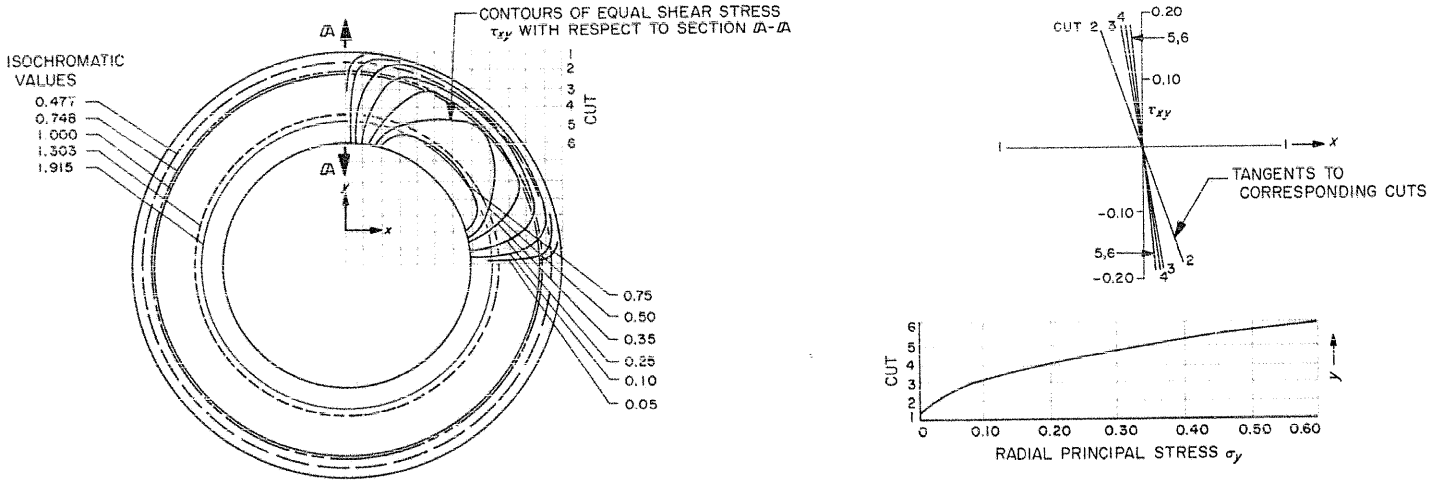

(b) FIXED TUBULAR GRAIN, 150 psi

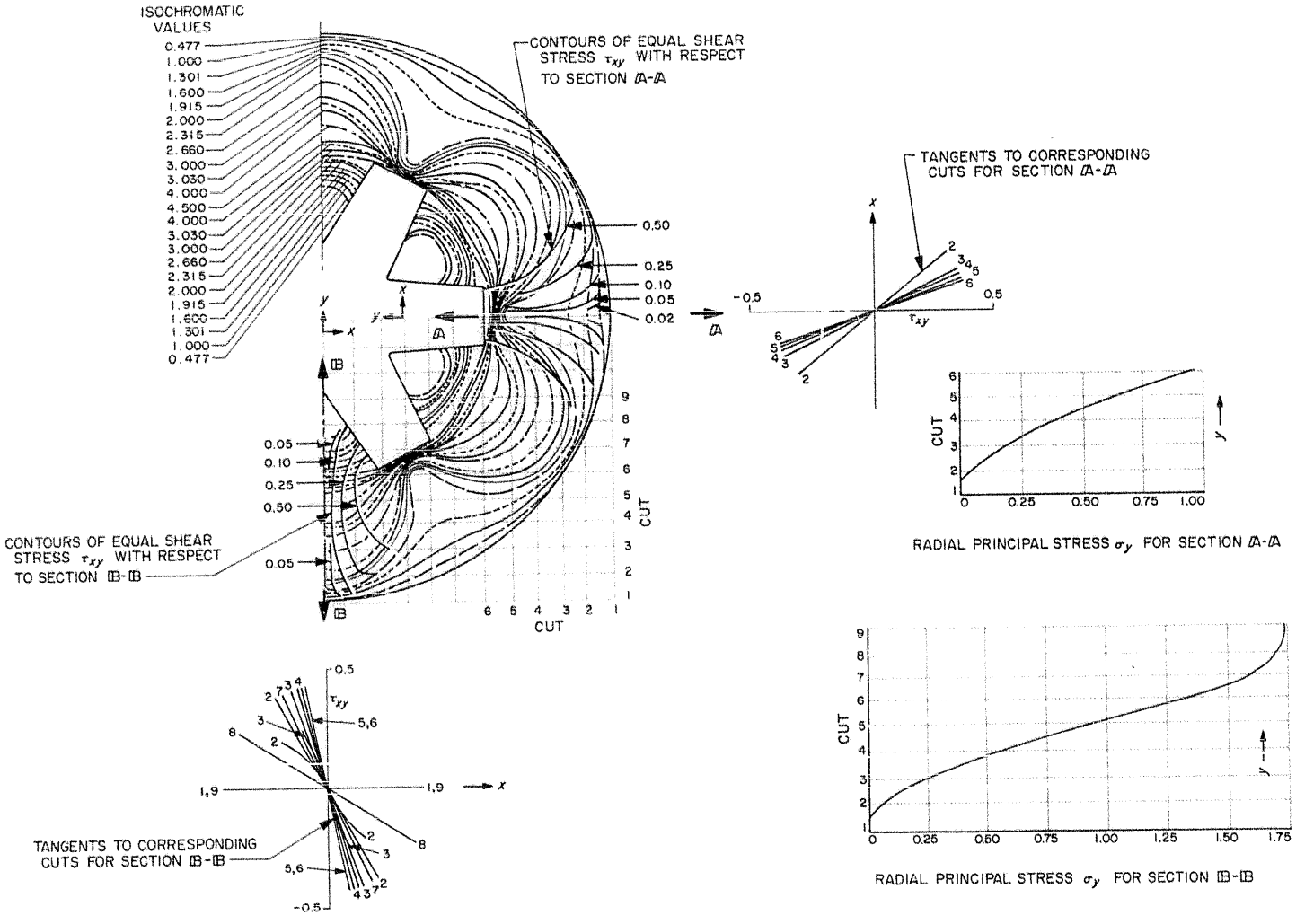

(d) FIXED STAR GRAIN, 150 psi

Figure 18 (Cont'd)

Table 2. Reduction of principal stresses to principal strains

Equations: $\varepsilon_1 = \frac{\sigma_1}{E} - \mu\frac{\sigma_2}{E}$; $\varepsilon_2 = \frac{\sigma_2}{E} - \mu\frac{\sigma_1}{E}$ for birefringent coating, $E = 410$ psi $\mu = 0.46$

Free tubular grain; 60 psi

	fringe orders			(in./in.) (fringe order/psi)		(in./in.) × 15.9	
Cut	$\sigma_1 - \sigma_2$ $\sigma_\theta - \sigma_r$ $\sigma_x - \sigma_y$	σ_2 σ_r σ_y	σ_1 σ_θ σ_x	ε_2	ε_1	ε_2	ε_1
1	0.45	0	0.45	−0.0005	0.0010	−0.008	0
2	0.81	−0.02	0.79	−0.0009	0.0019	−0.015	0.031
3	0.91	−0.11	0.80	−0.0012	0.0020	−0.018	0.033
4	1.05	−0.19	0.86	−0.0014	0.0023	−0.022	0.037
5	1.45	−0.32	1.13	−0.0020	0.0031	−0.033	0.050
6	1.96	−0.49	1.47	−0.0028	0.0040	−0.045	0.064

Fixed tubular grain; 150 psi

Cut	$\sigma_1 - \sigma_2$	σ_2	σ_1	ε_2	ε_1	ε_2	ε_1
1	0.30	0	0.30	−0.0003	0.0007	−0.005	0.012
2	0.75	−0.03	0.72	−0.0009	0.0017	−0.014	0.028
3	1.18	−0.10	1.08	−0.0014	0.0027	−0.023	0.044
4	1.28	−0.23	1.05	−0.0017	0.0028	−0.028	0.045
5	1.94	−0.40	1.54	−0.0027	0.0042	−0.043	0.067
6	2.30	−0.59	1.71	−0.0034	0.0048	−0.054	0.077

Free star grain; Section B; 60 psi

Cut	$\sigma_1 - \sigma_2$	σ_2	σ_1	ε_2	ε_1	ε_2	ε_1
1	0.85	0	0.85	−0.0010	0.0020	−0.015	0.033
2	1.22	−0.04	1.18	−0.0014	0.0029	−0.023	0.047
3	1.50	−0.21	1.29	−0.0020	0.0034	−0.031	0.054
4	1.92	−0.44	1.48	−0.0027	0.0041	−0.043	0.065
5	2.31	−0.75	1.56	−0.0035	0.0046	−0.057	0.074
6	1.92	−1.12	0.80	−0.0036	0.0032	−0.058	0.051
7	0.73	−1.43	−0.70	−0.0027	−0.0001	−0.043	−0.001
8	0.25	−1.46	−1.21	−0.0022	−0.0013	−0.035	−0.021
9	0	−1.46	−1.46	−0.0019	−0.0019	−0.031	−0.031

Free star grain; Section A; 60 psi;

Cut	$\sigma_1 - \sigma_2$	σ_2	σ_1	ε_2	ε_1	ε_2	ε_1
1	0.51	0	0.51	−0.0006	0.0012	−0.009	0.020
2	0.70	−0.03	0.67	−0.0008	0.0016	−0.013	0.026
3	0.86	−0.15	0.71	−0.0012	0.0019	−0.018	0.030
4	1.15	−0.31	0.84	−0.0017	0.0024	−0.027	0.038
5	1.55	−0.55	1.00	−0.0025	0.0031	−0.039	0.048
6	1.90	−0.86	1.04	−0.0033	0.0035	−0.052	0.056

Fixed star grain; Section B; 150 psi

Cut	$\sigma_1 - \sigma_2$	σ_2	σ_1	ε_2	ε_1	ε_2	ε_1
1	0.20	0	0.20	−0.0002	0.0005	−0.028	0.008
2	2.10	−0.06	2.04	−0.0024	0.0050	−0.039	0.080
3	2.70	−0.26	2.44	−0.0033	0.0060	−0.054	0.099
4	4.00	−0.55	3.45	−0.0052	0.0090	−0.083	0.143
5	4.25	−0.94	3.31	−0.0060	0.0091	−0.095	0.145
6	2.45	−1.34	1.11	−0.0045	0.0042	−0.072	0.067
7	2.30	−1.60	0.70	−0.0046	0.0035	−0.074	0.056
8	0.41	−1.71	−1.30	−0.0027	−0.0012	−0.043	−0.019
9	0	−1.74	−1.74	−0.0023	−0.0023	−0.036	−0.036

Fixed star grain; Section A; 150 psi

Cut	$\sigma_1 - \sigma_2$	σ_2	σ_1	ε_2	ε_1	ε_2	ε_1
1	0.10	0	0.10	−0.0001	0.0002	−0.017	0.004
2	1.00	−0.04	0.96	−0.0011	0.0024	−0.018	0.038
3	1.31	−0.20	1.11	−0.0017	0.0029	−0.027	0.046
4	1.44	−0.42	1.02	−0.0022	0.0030	−0.034	0.047
5	1.55	−0.68	0.87	−0.0026	0.0029	−0.042	0.046
6	2.60	−0.97	1.63	−0.0042	0.0051	−0.067	0.081

tal observations for the strain distribution corresponding to internal pressurization of a tubular grain. It is noted that the theoretical prediction of strains would require that the specimen begin to blanch on the interior surface. This was not confirmed by visual inspection. Thus, for a free standing tubular grain at the test pressure, it is shown that the theoretical prediction (Ref 2) is conservative by about 100%. For the contained tubular grain the circumferential strain agreed rather well; however, the radial strain predicted by theory was about 1000% conservative. It is noted that, in the experiment, direct contact between the grain and metal cylinder was prevented by a film of grease. This film was intended to create an experimental plane stress condition.

Figure 20 illustrates the radial strain distributions across a star tooth (Section B) and across the web (Section A). For Section B the point of interest is at Cut 5 located in the interior of the grain. This point exhibited the largest of strains. The high strain concentration points at the star point fillets were not examined because a less general experiment will be performed for that purpose. In comparing Figure 20 to Figure 19 for web strains, it is noted that the corresponding circumferential strains have about the same maximum magnitude but the star grain has a much steeper gradient for 150 psi. The maximum radial strains for the star configuration are somewhat higher than for the corresponding tubular configuration. Again a steeper gradient is observed.

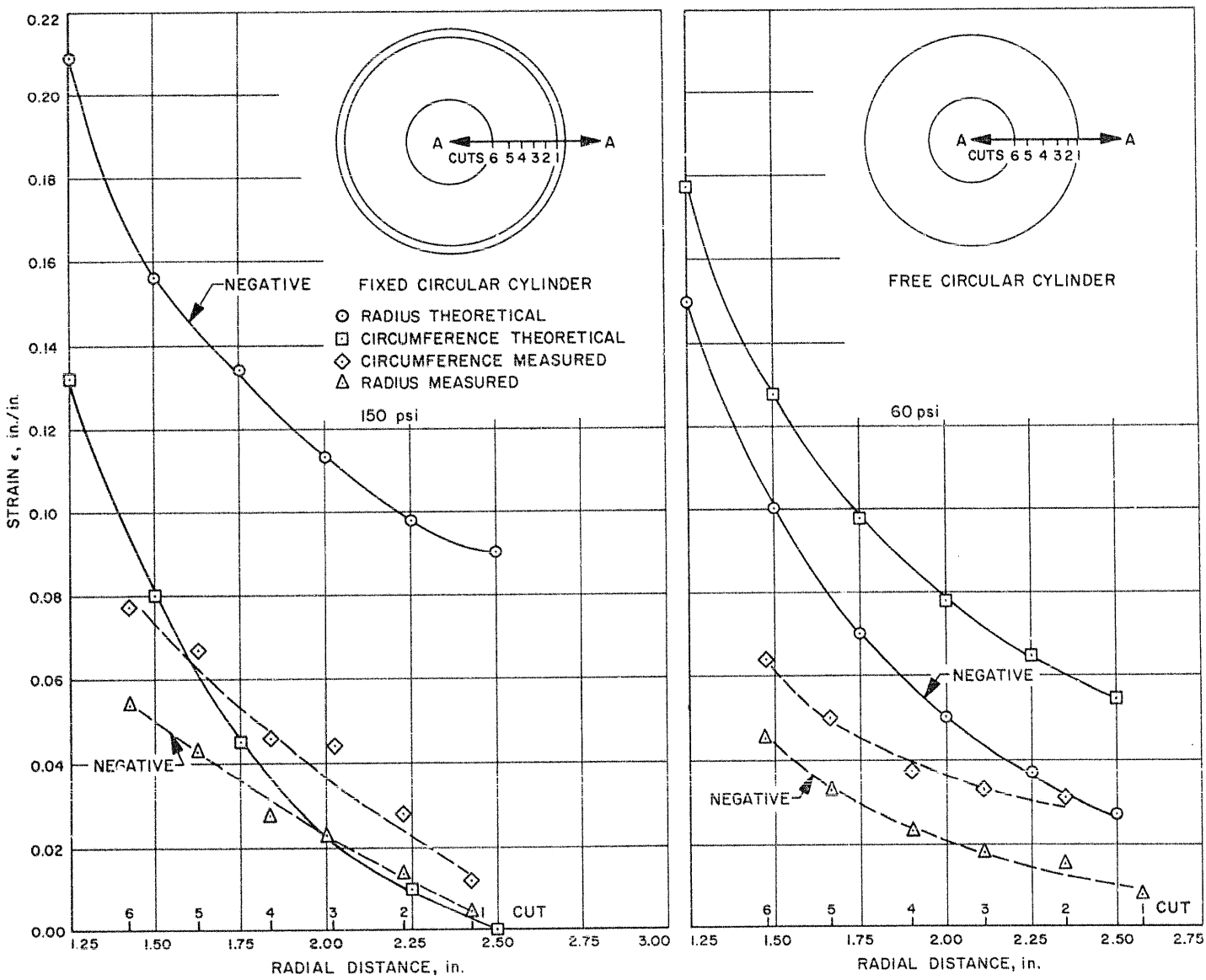

Figure 19. Discrepancies between small deformation elastic theory and experimental observations

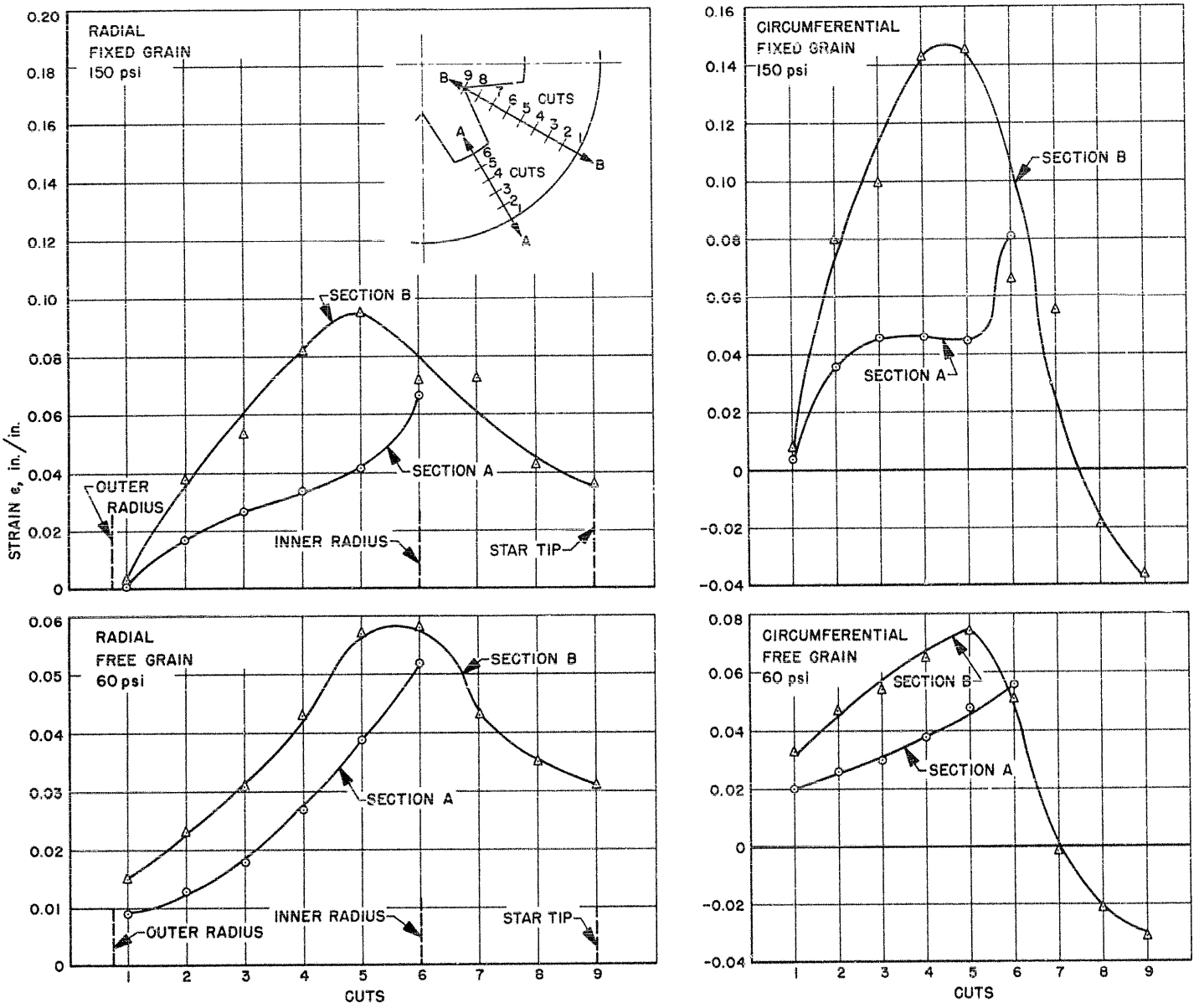

Figure 20. Radial and circumferential strain distributions of the star configuration

D. Polymer Degradation Mechanisms

J. D. Ingham and N. S. Rapp

The thermal degradation of polymers is being studied to determine the mechanisms of chemical interactions and to investigate the feasibility of developing nondestructive chemical methods for monitoring the extent of degradation and determining the storage life of solid propellants on the basis of structural chemical changes. For the present work, an uncrosslinked polyurethane analog of the current urethane propellant binders has been prepared for polyoxypropylene glycol (PPG) and toluene-2,4-diisocyanate (TDI). Ultimately, the relative susceptibilities of the ether and urethane linkages, to bond scission and branching, will be studied in vacuum, under inert and oxidative atmospheres, and in the presence and absence of additives.

1. Preparation of Polymer and Preliminary Experiments

Before use, the TDI was distilled and the PPG was heated to 100°C and sparged with dry nitrogen for 2

hours. The catalyst (ferric acetylacetonate, 0.02 wt % of polymer) was dissolved in the TDI, which was then added to the polypropylene glycol (NCO/OH mole ratio of 1.05) and cured for 70 hours at 60°C. The polymer was prepared in a dry box under nitrogen (relative humidity 2.5%). After curing, it was dissolved in benzene and stored in the dry box. The intrinsic viscosity in benzene was 0.71 dl/gm. This is higher than that reported previously for a similar polymer (Ref 3); however, the PPG used may have contained less monofunctional hydroxyl impurity. For example, the PPG of Reference 3 contained 1.1×10^{-5} moles/gm of carbonyl, very likely present as terminal acetoxyl (Ref 4); whereas, carbonyl was not detected in the PPG used here.

Intrinsic viscosities $[\eta]$ were measured using benzene solutions in Zhukov viscometers at 25 $\pm$0.02°C. Unless indicated otherwise, a limiting slope constant, K', of 0.39 was assumed and $[\eta]$ calculated from

$$\frac{\eta_{sp}}{C} = [\eta] + K'[\eta]^2 C$$

from a measurement at one concentration of <2 gm/dl. The value of K' of 0.39 was taken from the data of Reference 3 and verified for unfractionated, undegraded polymer. Intrinsic viscosities calculated in this fashion are relatively insensitive to moderate variations in K' at low polymer concentrations.

For infrared measurements, films of the polymer were deposited on sodium chloride plates, and the spectra were obtained before and after heating in air and nitrogen atmospheres. There was a small increase at 2.85 to 2.91μ (hydroxyl or amine) and a small decrease at 3.05μ (urethane hydrogen) after heating 14 days at 80°C. After a total heating period of 40 days no further qualitative spectral changes were observed. The spectrum of a bulk sample heated under nitrogen at 245°C for 24 hours indicated scission of the urethane linkage to give hydroxyl or amine and possibly unsaturated terminal groups. Solvents may affect chain scission by acting as urethane dissociation catalysts, by altering the relative rates of reactions of different orders, or by reacting with the polymer or degradation products; however, some effort will be devoted to degradative studies of benzene solutions, since an understanding of solvent effects could provide insight into the degradative processes. In addition, for certain experiments an inert solvent would improve tractability and allow better control of reactant concentrations and sample conditions.

To investigate the effects of solvents as media for carrying out degradative studies, two polymer samples were sealed in Zhukov viscometers in the presence of air, one as a 2.85 gm/dl benzene solution and the other a 2.65 gm/dl carbon tetrachloride solution, and placed in the 60°C bath. The benzene solution had an $[\eta]$ of 0.71 and a K' of 0.38 at 25°C determined by extrapolation of η_{sp}/C vs C to infinite dilution. At 60°C using a K' of 0.38, the initial viscosity was 0.69, decreasing to 0.16 after 120 days. The relative decrease is qualitatively the same as that found for samples degraded in bulk at 80°C, indicating that benzene has little effect on the degradation. For the carbon tetrachloride solution, $[\eta]$ at 25°C was 0.63 and K' was 0.49. At 60°C the initial value of $[\eta]$ was 0.40, presumably because degradation had occurred on standing overnight before being placed in the bath. It decreased to 0.040 after 21 days at 60°C.

Samples are being heated at 80°C to determine qualitatively the effects of oxygen and water on degradation of the bulk polymer samples in closed flasks under dry nitrogen, dry air, and water-saturated nitrogen. At intervals, polymer is withdrawn for intrinsic viscosity measurements utilizing an appropriate gas purge during sample withdrawal. Results are shown in Figure 21. Although these data suffer from the limitations of uncontrolled sample thickness, and variable oxygen and water vapor pressures, they show that bond scission is much more rapid in the presence of oxygen. Furthermore, these changes occur at moderate temperatures. It appears that the initial degradation rate is higher in the absence of oxygen if water is present. It may be that a small amount of moisture reacts with excess isocyanate that would ordinarily be used up in chain extension during simultaneous scission. The polymer is obviously very susceptible to oxidation.

To obtain preliminary data on the effects of ferric acetylacetonate (FeAA) and ammonium perchlorate (AP), in inert and oxidative atmospheres, a series of bulk polymer samples were heated in sealed tubes at temperatures of 40 and 80°C for 30 days. Intrinsic viscosities were then measured and are given in Table 3. FeAA promotes marked degradation except at 40°C in the absence of oxygen. Water-saturated air with no FeAA gives the most bond scission at 80°C, but apparently none at 40°C. With ammonium perchlorate in the presence of water-saturated air, the intrinsic viscosity decreased to 0.56 at 40°C and to 0.45 at 80°C; the latter value is comparable with 0.50 obtained under nitrogen and is much higher than the viscosity obtained when ammonium perchlorate was absent (0.047), indicating that perchlorate may exert a stabilizing effect under certain conditions.

Extensive data on degradation of uncrosslinked TDI–PPG polymer in solutions in the presence of additives

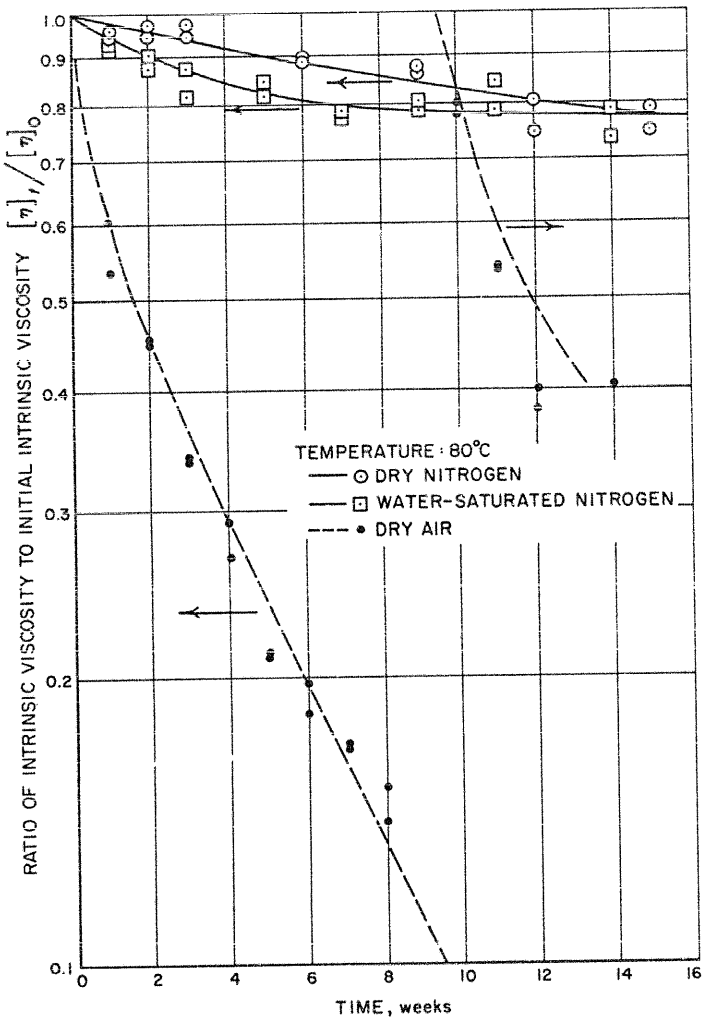

Figure 21. Degradation of polyoxypropylene-polyurethane in nitrogen, water-saturated nitrogen, and dry-air atmospheres

such as peroxide, water, potassium hydroxide, sulfuric acid, FeAA, and ammonium perchlorate are given in References 5, 6, and 7. Although quantitative comparisons are not possible, because of differences in conditions, the results are in qualitative agreement with the present work. The data obtained (Ref 7) for degradation in the presence of ammonium perchlorate did not show a significant stabilizing effect; however, no air or water was present and the solvent used was dimethylformamide, which promoted marked degradation.

2. *Degradation of Polymers in Vacuum and Investigation of Products*

A polymer sample weighing 0.35 gm was heated under vacuum in a flask, to which a capillary manometer was attached, for 24 hours at 60°C, 24 hours at 80°C, and 17 hours at 100°C. There was no pressure increase, and the intrinsic viscosity had not changed. Therefore, studies at 200°C were initiated with the ultimate objective of determining the degradation products and some features of the mechanism of degradation without the complications of oxidative reactions or catalysts. Lower temperatures and longer times will be used in later studies to obtain an understanding of degradative changes at ambient conditions.

After evacuating and degassing for 1 hour at 80°C, 1 gm polymer samples were sealed in tubes fitted with breakseals and then degraded at 203 ±3°C for 24 hours. Mass spectrographic analysis of the vapor over the samples showed the presence of CO_2 and trace amounts of other component(s) with mass peaks at 43 and 58 for samples heated at 150 and 200°C. Since the parent peak for acetone is 43 and that of propylene oxide and acetaldehyde appears at 58, it is probable that one or a combination of these is present. Components other than carbon dioxide could not be detected by vapor phase chromatography.

The tube was attached to the inlet system of the Consolidated chromatographic apparatus, and the vapor phase condensed in the inlet valve in vacuum and analyzed for CO_2 on a 6-foot silica gel (Fisher, 35–60 mesh) column at 90°C. Calibrations were carried out by injection of known amounts of CO_2 before and after sample analysis.

From a typical plot of CO_2 injected vs peak height shown in Figure 22, it appears that the precision of CO_2 analyses is within ±5%. Since detector response varies over a period of time even at constant operating conditions, permanent calibration curves are not practical. The polymer samples were dissolved in acetic acid and analyzed for amine by titration to the toluene-2,4-diamine end-point with perchloric acid dissolved in acetic acid (Refs 8, 9). Because of the small sample and indistinct end-points, results were semi-quantitative; however, they indicate the formation of amines. Initial data are given in Table 4.

It appears that insufficient CO_2 (0.016 meq/gm or ≈1.6 mole % of CO_2 initially present as urethane) was evolved to account for the number of linkages broken as indicated by the decrease from 0.715 to 0.340 in intrinsic viscosity, which could correspond to ≈6% urethanes ruptured. It is possible that the molecular weight distribution of the degraded polymer changed in such a way as to make any estimate of cuts from viscosity measurements unreliable, or that the source of some of the CO_2 may be auto-oxidative degradation of ether bonds,

Table 3. Effect of ferric acetylacetonate and ammonium perchlorate on the degradation of polyoxypropylene-polyurethane in the presence of oxygen and water vapor

Additive[a]	Atmosphere	Degradation temperature, °C (30 days)	Intrinsic viscosity, dl/gm	Nominal extent[b] degraded, %			
				<1	1 to 5	5 to 20	>>20
—	Nitrogen	40	0.70				
—	Nitrogen	80	0.49				
—	Water + air	40	0.74				
—	Water + air	80	0.05				
Ferric acetylacetonate	Air	40	0.27				
Ferric acetylacetonate	Water + air	80	0.09				
Ferric acetylacetonate	Nitrogen	40	0.66				
Ferric acetylacetonate	Nitrogen	80	0.25				
Ferric acetylacetonate	Water + air	40	0.13				
Ferric acetylacetonate	Water + air	80	0.09				
Ammonium perchlorate	Water + air	40	0.55				
Ammonium perchlorate	Water + air	80	0.44				

[a] The sample sizes were 0.08 gm to which 0.005 gm of additive was added in acetone which was removed by evaporation.

[b] The ranges represent the percent of urethane linkages that could have broken, assuming the molecular weight distribution has not changed greatly during degradation and that branching has not occurred.

or that some of it may have recombined with the polymer on cooling prior to analysis. From the limited data obtained, it appears that the only volatile product found in readily detectable amounts is carbon dioxide and that the degradation possesses random scission features as opposed to chain unzipping to give large amounts of low-molecular-weight fragments.

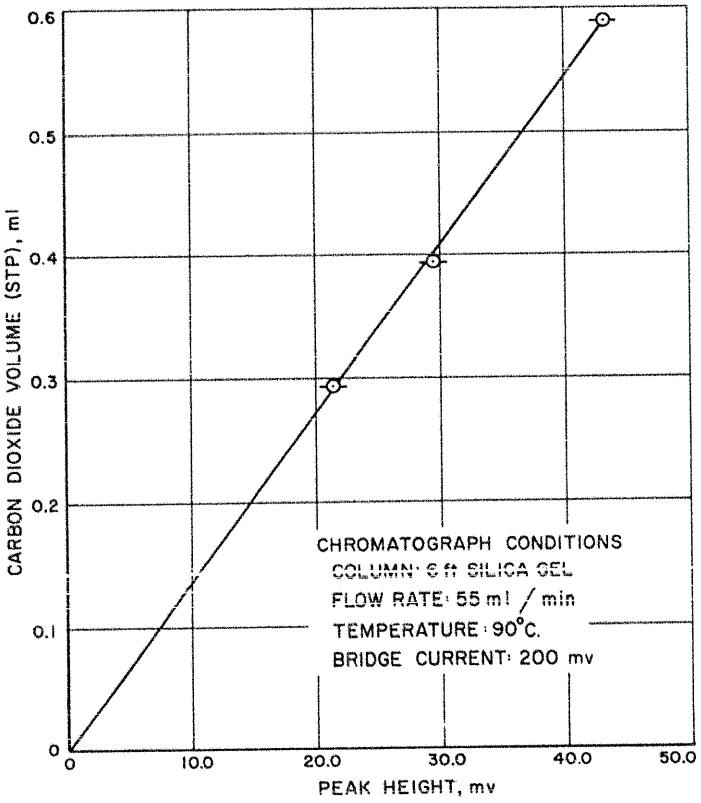

Figure 22. Volume of carbon dioxide vs peak height by vapor phase chromatography

Table 4. Intrinsic viscosity, amine, and carbon dioxide analyses of polyoxypropylene glycol-toluene diisocyanate polymer after heating under vacuum at 203°C for 24 hours[a]

Intrinsic viscosity[b]		Amine, meq/gm × 10[3]	Carbon dioxide, meq/gm × 10[3]
[η], dl/gm	Slope constant K′		
0.38	0.36	9	—
0.36	0.35	9	—
0.38	0.35	6	—
0.35	0.35	6	—
0.38	0.35	6	—
0.35	0.35	2	15
0.32	0.35	3	15
0.32	0.34	2	13
0.30	0.34	9	18
0.33	0.35	3	19
0.30	0.35	2	—
0.30	0.35	2	18

[a] The polymer initially had an intrinsic viscosity of 0.715 dl/gm and contained approximately 1 meq/gm of urethane linkages.

[b] The large deviation in intrinsic viscosity is due to sample differences rather than measurement error, possibly caused by temperature variations (±3°C) and gradients. An oil bath with temperature regulation very close to 200°C was used for the first five samples and an air bath at 203 ±3°C for the others.

It is evident that the degradation of polyoxypropylene glycol-toluene diisocyanate condensation polymers, even in the absence of an oxidative atmosphere and catalytic additives, may be exceedingly complex. Recent publications (Refs 10, 11, and 12) suggest that a minimum of one equivalent of CO_2 per equivalent of urethane scission would be expected, but the amount of CO_2 found per cut could be much more; also, numerous reactions leading to branching can occur. In addition, scission at bonds other than the urethane, such as labile peroxide or others, has not been excluded. Thus, in order to establish the mechanism of PPG–TDI polymer degradation, it will be necessary to determine number average molecular weights, weight average molecular weights, molecular weight distributions, carbon dioxide evolution, and other chemical changes as a function of time and temperature. Because of the small concentration of functional groups formed (which may be less than 0.01 meq/gm), much further work on the development of analytical methods will be required. In addition, a reasonably rapid means of fractionating the polymer is needed. Development of a method utilizing elution column chromatography from an inert substrate is in progress.

E. Homogeneity of Polyurethane Propellants

A. J. Havlik and J. Moacanin

To prepare homogeneous composite propellants, the dispersion and chemical uniformity must be maintained during mixing, casting, and curing; if meaningful test results are to be obtained, this uniformity must also be maintained during sampling and testing.

For a study of a given propellant system, therefore, preparative conditions which affect the homogeneity of the grain and those which will minimize changes during testing will have to be determined.

Previously (Ref 13), an investigation was performed on the importance to the homogeneity of composite propellant mixing, casting, mold design, temperature and duration of cure, and the preparation and handling of test specimens. It was found that the atmosphere to which the propellant is exposed and a wall effect related to the thermal history during cure can be major factors which influence the homogeneity. While the wall effect is limited to the cure period, the atmosphere effect is manifest during casting, curing, and handling of test specimens. In particular, it was found that exposure of the propellant slurry to the normal ambient air during casting increased the tensile strength, S_m, by 40% (80 to 125 psi) at 77°F, as compared to charges cast under vacuum. This study has been extended by investigating the effect of the nature of the atmosphere present during casting on the mechanical properties of JPL X-600 and X-500 polyurethane propellants. Two series of propellant batches were prepared and tested following the procedure described in References 13 and 14. The compositions of these propellants are given in Table 5.

The tensile strengths, S_m, and elongations at maximum stress, e_m, for the X-600 charges cast under dry nitrogen, dry oxygen (dew points < -50°F), water-saturated nitrogen, and water-saturated air are summarized in Table 6. Significant differences in mechanical properties are observed for charges cast under dry and wet atmospheres.

Table 5. Compositions of X-600 and X-500 propellants[a]

Ingredients	Weight, %		
	X-600	X-500E, A	X-500E, B
Ammonium perchlorate, ground	56.0	56.0	56.0
Ammonium perchlorate, unground	24.0	24.0	24.0
Lithium perchlorate	0.095	0.090	—
Polypropylene gylcol 2025	15.3	13.2	13.3
P I (Estane)	—	5.127	5.151
P II prepolymer	2.55	—	—
1, 2, 3-trimethylol propane	0.101	0.088	0.088
BLE (antioxidant)	0.26	0.26	0.26
Ferric acetylacetonate	0.033	0.033	0.033
2, 4-toluene diisocyanate	1.64	1.16	1.17

[a] Cured 91¼ hr at 180°F.

Table 6. Tensile strength and elongation at maximum stress[a] for a X-600 propellant[b] cast under various atmospheres

Location of sample in mold	Dry gases				Water saturated gases			
	Oxygen		Nitrogen		Nitrogen		Air	
	S_m, psi	e_m	S_m, psi	e_m	S_m, psi	e_m	S_m, psi	e_m
Top	66	1.04	61	1.17	123	0.48	125	0.46
Bottom	73	0.83	66	0.92	130	0.45	134	0.45
Average	70	0.99	64	1.04	127	0.47	129	0.46

[a] Average of eight tensile bars (wall bars omitted); tested at 77°F with a jaw separation rate of 2 in./min.

[b] Binder parameters: $NCO/(OH + NH_2) = 1.12$; $NH_2/(OH + NH_2) = 0.047$; $OH_{triol}/(OH + NH_2) = 0.112$.

The average S_m values of 67 psi for the dry-cast and 128 psi for the wet-cast are comparable to the previously reported values for vacuum (70 psi) and air-cast charges (relative humidity = 30 to 50%; 125 psi), respectively, showing that moisture rather than oxygen or nitrogen caused an increase in the S_m values.

Similar data for two X-500 formulations are given in Table 7. Again, differences in mechanical properties are observed between charges cast under dry and wet nitrogen. As with the X-600 propellants, the specimens obtained from the wet-cast charges have higher S_m (104 and 99 vs 60 and 50 psi), and lower e_m (0.46 and 0.40 vs 0.70 and 0.83) than those from the dry-cast.

Moisture, present during casting, not only influenced the magnitude of S_m but greatly altered the stress–strain behavior as illustrated in Figure 23 for both the X-600 and X-500 propellants. Wet-cast propellants exhibit a high S_m and a rapid descent to break, while dry-cast propellants are characterized by a low S_m and a gradual decrease in strength to break.

Table 7. Tensile strength and elongation at maximum stress[a] for X-500 propellants[b] cast under dry or wet nitrogen atmospheres

Location of sample in mold	Formulation A with Li^+				Formulation B w/o Li^+			
	Dry N_2		Wet N_2		Dry N_2		Wet N_2	
	S_m, psi	e_m	S_m, psi	e_m	S_m, psi	e_m	S_m, psi	e_m
Top	58	0.76	97	0.48	49	0.95	96	0.42
Bottom	62	0.63	104	0.44	52	0.71	102	0.39
Average	60	0.70	104	0.46	50	0.83	99	0.40

[a] Average of 10 tensile bars except only four tensile bars for the bottom of the X-500 without Li^+.

[b] Binder parameters: NCO/OH = 1.12; OH_{triol}/OH = 0.103; cured 91¼ hr at 180°F.

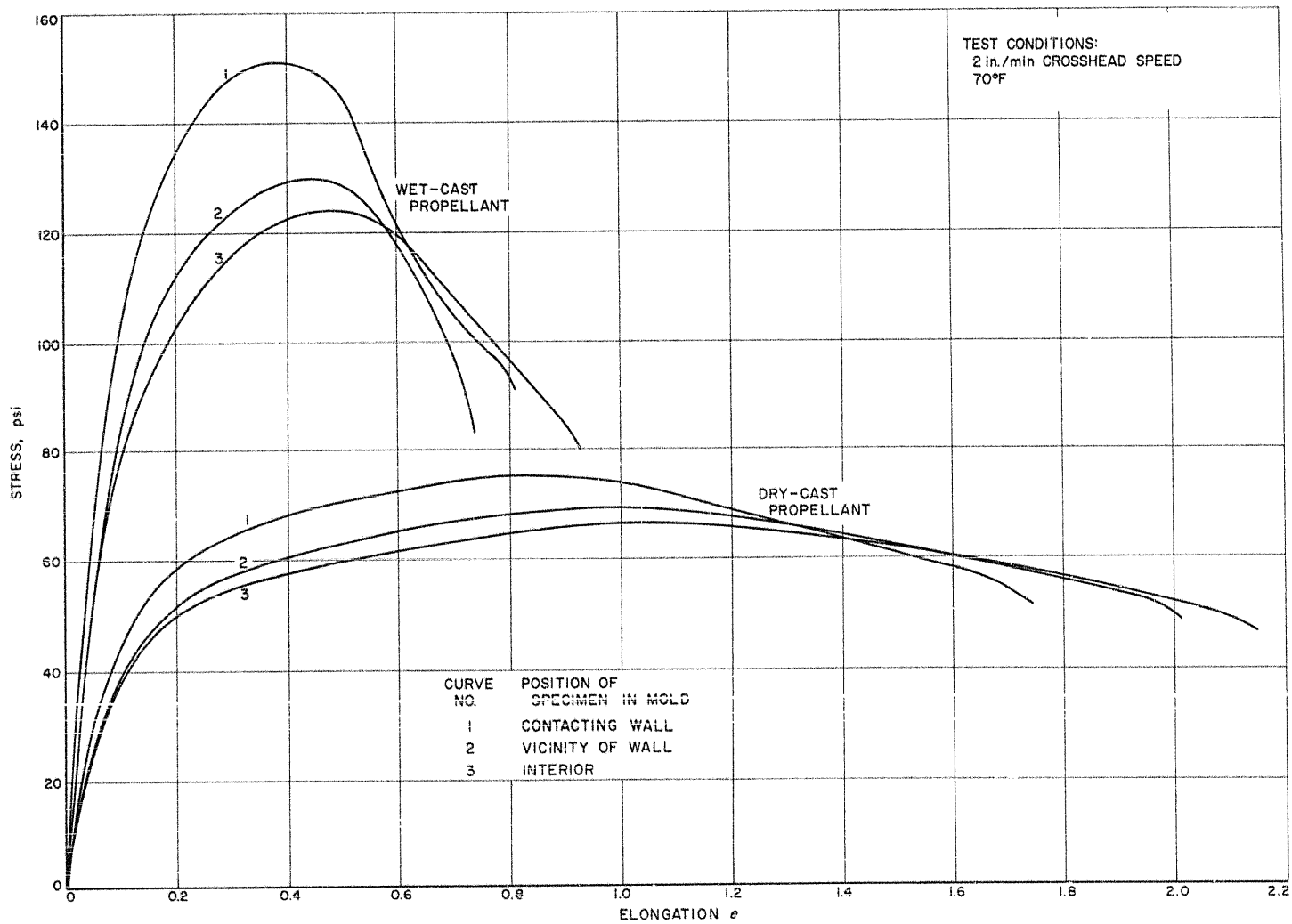

Figure 23. Comparison of stress–strain for wet- and dry-cast propellant as a function of position in the mold

Although significant differences in mechanical properties resulted from exposure to moisture during casting, similar exposure to moisture during consolidation had no effect. This is to be expected since a relatively small surface area is in contact with the gas during consolidation.

Further inspection of Tables 6 and 7 shows that there is a significant difference (t-test, 99% level) in the S_m values between the top and bottom layers for each of the charges. These differences cannot be due to an atmosphere effect during cure (Ref 13), since tightly covered molds were used for these experiments. The locations of the tensile specimens in a cured grain are shown in Figure 24, and the S_m values are given for the X-600 charge cast under wet nitrogen. The top specimens away from the walls (Nos. 2 through 9) have an average S_m value of 123 psi, while specimens with the maximum wall contact (Nos. 11 and 20) have an average S_m value of 157 psi, indicating that S_m increases with increased contact of the tensile specimens with the walls of the molds. This effect is attributed to the influence of the geometry of the molds on the thermal histories of the specimens (Ref 13). Similar trends were observed for the other charges.

A top to bottom difference is observed in the e_m values for the dry-cast but not the wet-cast propellants. Moisture, when present during casting, appears predominant in influencing the level of S_m values.

The thermal effect on the cure is also manifest in the stress–strain behavior as illustrated in Figure 23. For both

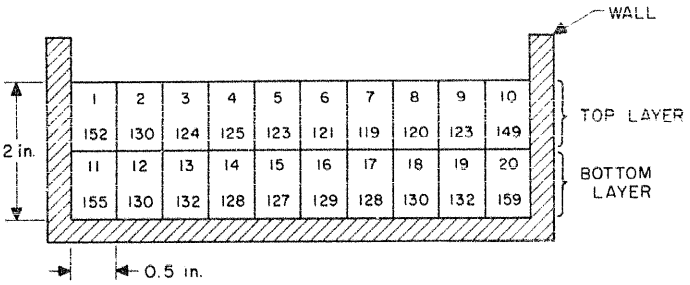

Figure 24. Tensile specimen locations and tensile strength, S_m, for wet-cast Propellant I

wet and dry charges: Curves 1 are characteristic of specimens which were in contact with the walls; Curves 2—close to, but not in contact with, the walls; and Curves 3—in the interior of the mold.

It is clear from the preceding results that the moisture and wall effects are present in both X-600 and X-500 propellants with or without lithium. Therefore, these effects appear to be general to the polyurethanes and are not peculiar to the differences between X-600 and X-500 propellants. The question, whether the moisture effect should be attributed to a modification in the cure of the binder or a change in the adhesion between oxidizer and binder, will be studied as a part of other JPL projects.

The experimentation Phase 3 of the homogeneity study has been completed, and the project will be terminated.

References

1. Surland, C. C. and Jacobs, J. M., "Measurement of Triaxial Strains from Hydrostatic Stress," *Bulletin of the 18th JANAF Meeting on Physical Properties of Propellants*, Solid Propellant Information Agency, The Johns Hopkins University, Silver Spring, Maryland, June 1959.

2. Schapery, R. A. and Stimpson, L. D., *Fundamental Studies Relating to Systems Analysis of Solid Propellants*, Progress Report No. 1, GALCIT 101, Guggenheim Aeronautical Laboratory, California Institute of Technology, Pasadena, California, January 15, 1959.

3. Moacanin, J., "Diisocyanate-Linked Polymers. I. Dilute-Solution Properties of Toluene Diisocyanate-Extended Polypropylene Glycol," *Journal of Applied Polymer Science*, Vol I, pp 272–282, 1959.

4. Simons, D. M. and Verbanc, J. J., "The Polymerization of Propylene Oxide," *Journal of Polymer Science*, Vol XLIV, pp 303–311, 1960.

5. *Combined Bimonthly Summary No. 61*, Jet Propulsion Laboratory, Pasadena, California, October 15, 1957 (Confidential).

6. *Combined Bimonthly Summary No. 67*, Jet Propulsion Laboratory, Pasadena, California, October 15, 1958 (Confidential).

7. *Combined Bimonthly Summary No. 68*, Jet Propulsion Laboratory, Pasadena, California, December 15, 1958 (Confidential).

8. Seaman, W. and Allan, E., "Acid-Base Titrations on Glacial Acetic Acid," *Analytical Chemistry*, Vol 23, pp 592–594, 1951.

9. Fritz, J. S., "Titration of Bases in Nonaqueous Solvents," *Analytical Chemistry*, Vol 22, pp 1028, 1029, 1950.

10. Dyer, E. and Osborne, D. W., "The Thermal Degradation of a Polythiolcarbamate," *Journal of Polymer Science*, Vol XLVII, pp 349–359, 1960.

11. Fletcher, M. A., Laksin, M. W., and Plant, S. G. P., "The Pyrolysis of Some Complex Urethans," *Journal of the Chemical Society*, pp 3898–3902, 1953.

12. Dyer, E. and Wright, G. C., "Thermal Degradation of Alkyl N-Phenylcarbamates," *Journal of the American Chemical Society*, Vol 81, pp 2138–2143, 1959.

13. *Research Summary No. 36-5*, Vol III, Jet Propulsion Laboratory, Pasadena, California, November 15, 1960 (Confidential).

14. *Research Summary No. 36-7*, Vol III, Jet Propulsion Laboratory, Pasadena, California, March 15, 1961 (Confidential).